

First edition  
2016-05-01

---

---

## Nanotechnologies — Characterization of cellulose nanocrystals

*Nanotechnologies — Caractérisation des nanocristaux de cellulose*



Reference number  
ISO/TR 19716:2016(E)



**COPYRIGHT PROTECTED DOCUMENT**

© ISO 2016, Published in Switzerland

All rights reserved. Unless otherwise specified, no part of this publication may be reproduced or utilized otherwise in any form or by any means, electronic or mechanical, including photocopying, or posting on the internet or an intranet, without prior written permission. Permission can be requested from either ISO at the address below or ISO's member body in the country of the requester.

ISO copyright office  
Ch. de Blandonnet 8 • CP 401  
CH-1214 Vernier, Geneva, Switzerland  
Tel. +41 22 749 01 11  
Fax +41 22 749 09 47  
copyright@iso.org  
www.iso.org

# Contents

Page

<b>Foreword</b> .....	<b>iv</b>
<b>Introduction</b> .....	<b>v</b>
<b>1 Scope</b> .....	<b>1</b>
<b>2 Terms and definitions</b> .....	<b>1</b>
<b>3 Symbols and abbreviated terms</b> .....	<b>2</b>
<b>4 Production of cellulose nanocrystals (CNCs)</b> .....	<b>3</b>
<b>5 Composition</b> .....	<b>6</b>
5.1 Chemical composition.....	6
5.2 Surface functional groups.....	7
5.2.1 Determination of sulfate half-esters.....	7
5.2.2 Determination of carboxylic acids.....	11
5.3 Degree of polymerization.....	12
5.4 Crystallinity.....	13
5.4.1 General.....	13
5.4.2 X-ray diffraction.....	14
5.4.3 Nuclear magnetic resonance.....	16
5.4.4 Vibrational spectroscopy.....	18
5.4.5 Crystallinity measurements for CNCs.....	18
5.5 Moisture content.....	20
5.6 Contaminants.....	20
5.6.1 General.....	20
5.6.2 Residual impurities derived from cellulosic biomass.....	21
5.6.3 Metal ions.....	21
5.6.4 Detection of contaminants by X-ray photoelectron spectroscopy.....	21
<b>6 CNC Morphology</b> .....	<b>22</b>
6.1 Distributions of length and cross-section from microscopy.....	22
6.1.1 General.....	22
6.1.2 Electron microscopy.....	23
6.1.3 Atomic force microscopy.....	25
6.1.4 Image analysis considerations.....	27
6.1.5 Microscopy size distributions for CNCs.....	27
6.2 Size measurement by dynamic light scattering (DLS).....	31
<b>7 CNC Surface characteristics</b> .....	<b>33</b>
7.1 Specific surface area.....	33
7.2 Surface charge.....	34
<b>8 Miscellaneous</b> .....	<b>35</b>
8.1 Thermal properties.....	35
8.2 Viscosity.....	38
<b>9 Concluding comments</b> .....	<b>38</b>
<b>Bibliography</b> .....	<b>40</b>

## Foreword

ISO (the International Organization for Standardization) is a worldwide federation of national standards bodies (ISO member bodies). The work of preparing International Standards is normally carried out through ISO technical committees. Each member body interested in a subject for which a technical committee has been established has the right to be represented on that committee. International organizations, governmental and non-governmental, in liaison with ISO, also take part in the work. ISO collaborates closely with the International Electrotechnical Commission (IEC) on all matters of electrotechnical standardization.

The procedures used to develop this document and those intended for its further maintenance are described in the ISO/IEC Directives, Part 1. In particular the different approval criteria needed for the different types of ISO documents should be noted. This document was drafted in accordance with the editorial rules of the ISO/IEC Directives, Part 2 (see [www.iso.org/directives](http://www.iso.org/directives)).

Attention is drawn to the possibility that some of the elements of this document may be the subject of patent rights. ISO shall not be held responsible for identifying any or all such patent rights. Details of any patent rights identified during the development of the document will be in the Introduction and/or on the ISO list of patent declarations received (see [www.iso.org/patents](http://www.iso.org/patents)).

Any trade name used in this document is information given for the convenience of users and does not constitute an endorsement.

For an explanation on the meaning of ISO specific terms and expressions related to conformity assessment, as well as information about ISO's adherence to the WTO principles in the Technical Barriers to Trade (TBT) see the following URL: [Foreword - Supplementary information](#)

The committee responsible for this document is ISO/TC 229, *Nanotechnologies*.

## Introduction

Cellulose nanomaterials, including cellulose nanocrystals (CNCs) and cellulose nanofibrils, are anticipated to have significant commercial impact. Cellulose nanocrystals are extracted from naturally occurring cellulose, primarily from wood and annual plants, by acid hydrolysis, or chemical or enzymatic oxidation.<sup>[1][2][3]</sup> Their production from cellulose sources, such as wood pulps makes them a candidate for use as a potentially non-toxic, biodegradable and sustainable nanomaterial. Furthermore, the recent demonstration of the feasibility of CNC production on a large scale and the availability of infrastructure for harvesting raw materials will facilitate their commercial development. CNCs and cellulose nanofibrils are produced in a number of countries on pilot, pre-commercial or commercial scales. Estimates of the market potential for cellulosic nanomaterials are as high as 35 million metric tons annually, depending on the predicted applications and the estimated market penetration.<sup>[4][5]</sup> Standards for characterization of CNCs are required for material certification to allow sustained commercial development and applications.

Cellulose nanocrystals are nanorods that have high aspect ratio, surface area and mechanical strength and assemble to give a chiral nematic phase with unique optical properties. They are smaller than cellulose nanofibrils and have a higher crystalline content. These properties, plus the ability to control CNC surface charge and chemistry for dispersion in a variety of matrices, lead to potential applications in many areas including nanocomposite materials, paints and adhesives, optical films and devices, rheology modifiers, catalysts and biomedical products. There are currently no International Standards for this emerging commercial nanomaterial, although an ISO/TC 229 project on terminology is in progress, a Canadian National Standard (CSA Z5100) was published in 2014 and two CNC reference materials were released in 2013. This Technical Report reviews information on sample preparation, data collection and data analysis/interpretation for the measurands that are predicted to be important for the development of commercial products containing CNCs. Information for the following CNC properties is included: composition (crystallinity, surface functional groups, degree of polymerization and contaminants), morphology as assessed by microscopy and light scattering methods, surface charge and specific surface area, viscosity and thermal stability. The Technical Report reviews various approaches that have been used for specific properties, but does not recommend standard methods or provide detailed information on the techniques. The coverage is restricted to CNCs as produced and does not extend to post-production modified CNCs or CNC-enhanced materials or products.



# Nanotechnologies — Characterization of cellulose nanocrystals

## 1 Scope

This Technical Report reviews commonly used methods for the characterization of cellulose nanocrystals (CNCs), including sample preparation, measurement methods and data analysis. Selected measurands for characterization of CNCs for commercial production and applications are covered. These include CNC composition, morphology and surface characteristics.

## 2 Terms and definitions

For the purposes of this document, the following terms and definitions apply.

### 2.1

#### **agglomerate**

collection of weakly or medium strongly bound particles where the resulting external surface area is similar to the sum of the surface areas of the individual components

Note 1 to entry: The forces holding an agglomerate together are weak forces, for example, van der Waals forces or simple physical entanglement.

Note 2 to entry: Agglomerates are also termed secondary particles and the original source particles are termed primary particles.

[SOURCE: ISO/TS 80004-2:2015, 3.3]

### 2.2

#### **aggregate**

particle comprising strongly bonded or fused particles where the resulting external surface area is significantly smaller than the sum of surface areas of the individual components

Note 1 to entry: The forces holding an aggregate together are strong forces, for example, covalent bonds, or those resulting from sintering or complex physical entanglement, or otherwise combined former primary particles.

Note 2 to entry: Aggregates are also termed secondary particles and the original source particles are termed primary particles.

[SOURCE: ISO/TS 80004-2:2015, 3.4]

### 2.3

#### **nanocrystal**

nano-object with a crystalline structure

[SOURCE: ISO/TS 80004-2:2015, 4.15]

### 2.4

#### **nanofibre**

nano-object with two external dimensions in the nanoscale and the third dimension significantly larger

Note 1 to entry: The largest external dimension is not necessarily in the nanoscale.

Note 2 to entry: The terms nanofibril and nanofilament can also be used.

## 2.5

### **nano-object**

discrete piece of material with one, two or three external dimensions in the nanoscale

Note 1 to entry: The second and third external dimensions are orthogonal to the first dimension and to each other.

[SOURCE: ISO/TS 80004-2:2015, 2.2]

## 2.6

### **nanorod**

solid nanofibre

[SOURCE: ISO/TS 80004-2:2015, 4.7]

## 2.7

### **nanoscale**

size range from approximately 1 nm to 100 nm

Note 1 to entry: Properties that are not extrapolations from a larger size will typically, but not exclusively, be exhibited in this size range. For such properties the size limits are considered approximate.

Note 2 to entry: The lower limit in this definition (approximately 1 nm) is introduced to avoid single and small groups of atoms from being designated as nano-objects or elements of nanostructures, which might be implied by the absence of a lower limit.

[SOURCE: ISO/TS 80004-2:2015, 2.1]

## 3 Symbols and abbreviated terms

For the purposes of this document, the following symbols and abbreviated terms apply.

AEC	anion-exchange chromatography
AFM	atomic force microscopy
BET	Brunauer-Emmett-Teller (method for determination of specific surface area)
CrI	crystallinity index (also CI)
CNC(s)	cellulose nanocrystal(s)
CP-MAS	cross polarization magic angle spinning
$d_h$	hydrodynamic diameter
DP	degree of polymerization
$D_t$	translational diffusion coefficient
DSC	differential scanning calorimetry
DLS	dynamic light scattering
$\epsilon$	dielectric constant
EM	electron microscopy
FE-SEM	field emission-scanning electron microscopy
FTIR	Fourier transform infrared spectroscopy



GLC	gas-liquid chromatography
ICP-MS	inductively coupled plasma-mass spectrometry
ICP-OES	inductively coupled plasma-optical emission spectroscopy
ID	isotope dilution
IR	infrared
$k$	Boltzmann constant
PI	polydispersity
ssNMR	solid state nuclear magnetic resonance
SEC	size exclusion chromatography
SEM	scanning electron microscopy
TEM	transmission electron microscopy
TEMPO	2,2,6,6-tetramethyl-1-piperidinyloxy free radical
TGA	thermogravimetric analysis
$U_E$	electrophoretic mobility
$\eta$	viscosity
XPS	X-ray photoelectron spectroscopy
XRD	X-ray diffraction

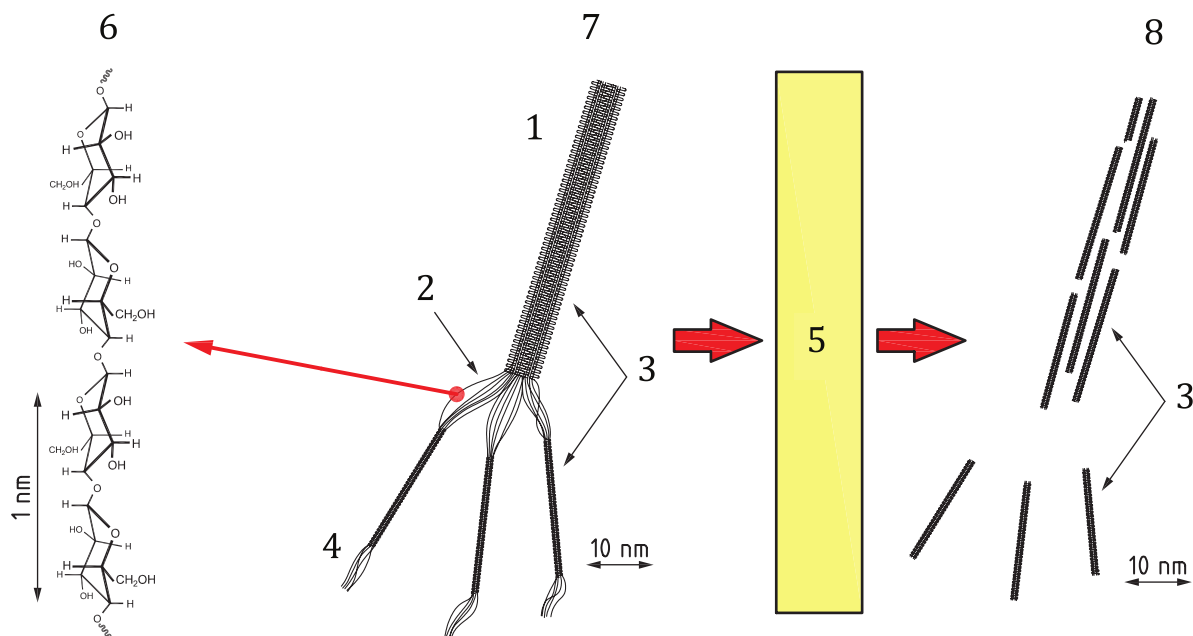
#### 4 Production of cellulose nanocrystals (CNCs)

Cellulose is a linear polysaccharide composed of anhydroglucose units linked by an oxygen atom between the C1 and C4 carbons of adjacent glucose rings. In cellulose biosynthesis individual, polysaccharide chains are assembled by an enzyme complex into an elementary fibril with stacked chains held together by hydrogen bonding. The number and organization of polymer chains is specific to the organism. These elementary fibrils are further assembled to give larger structures that contain ordered (crystalline), as well as disordered cellulose and other components that depend on the organism.

Cellulose nanocrystals are formed from one or more elementary fibrils and contain primarily crystalline and paracrystalline regions. CNCs have length and cross-sectional dimensions that depend on the cellulose source with typical aspect ratios between 5 and 50 and do not exhibit branching or network-like structures. The term nanocrystalline cellulose is synonymous with CNCs and the term nanowhiskers has also been used frequently in the literature. Cellulose nanofibrils are typically larger than CNCs and are branched, entangled and agglomerated structures. The nanofibrils have crystalline, paracrystalline and amorphous regions and can contain non-cellulosic components. They have cross-sections between 5 nm and 50 nm and aspect ratios that are greater than 50. An ISO/TC 229 project<sup>[6]</sup> aimed at standardizing the terminology for cellulose nanomaterials has recently been initiated.

Cellulose nanocrystals are produced from a variety of cellulose sources, primarily wood and other plants, but also algae, bacteria and tunicates.<sup>[2][3][7][8][9][10][11][12][13]</sup> Their extraction from cellulose-containing biomass begins with mechanical and/or chemical pre-treatment to remove non-cellulose components, reduce the particle size and increase the exposed surface area. This is followed by a hydrolysis or oxidation step that digests the more reactive amorphous cellulose and liberates CNCs from the larger cellulose fibrils (Figure 1). Acid hydrolysis with sulfuric acid is the most widely used method for CNC production in both research laboratories and pilot scale commercial facilities, although other

acids (e.g. hydrochloric, phosphoric, phosphotungstic) have also been employed.[2][3][7][8][9][14][15] In attempts to minimize the use of strong acids, a variety of other processes have also been examined including ultrasonication-assisted hydrolysis (with or without an iron chloride catalyst), enzymatic oxidation and ammonium persulfate oxidation.[16][17][18] After the acid hydrolysis or oxidation step, CNCs are purified by a combination of centrifugation or filtration and washing steps, followed by dialysis to remove residual salt and/or acids. A typical sequence for CNC production by acid hydrolysis is illustrated in [Figure 2](#).



**Key**

- 1 micro-fibril
- 2 disordered
- 3 crystalline
- 4 elementary fibrils
- 5 hydrolysis or oxidation
- 6 cellulose
- 7 cellulose fibril
- 8 cellulose nanocrystals

**Figure 1 — Cartoon description of the formation of CNCs from larger cellulose fibrils**

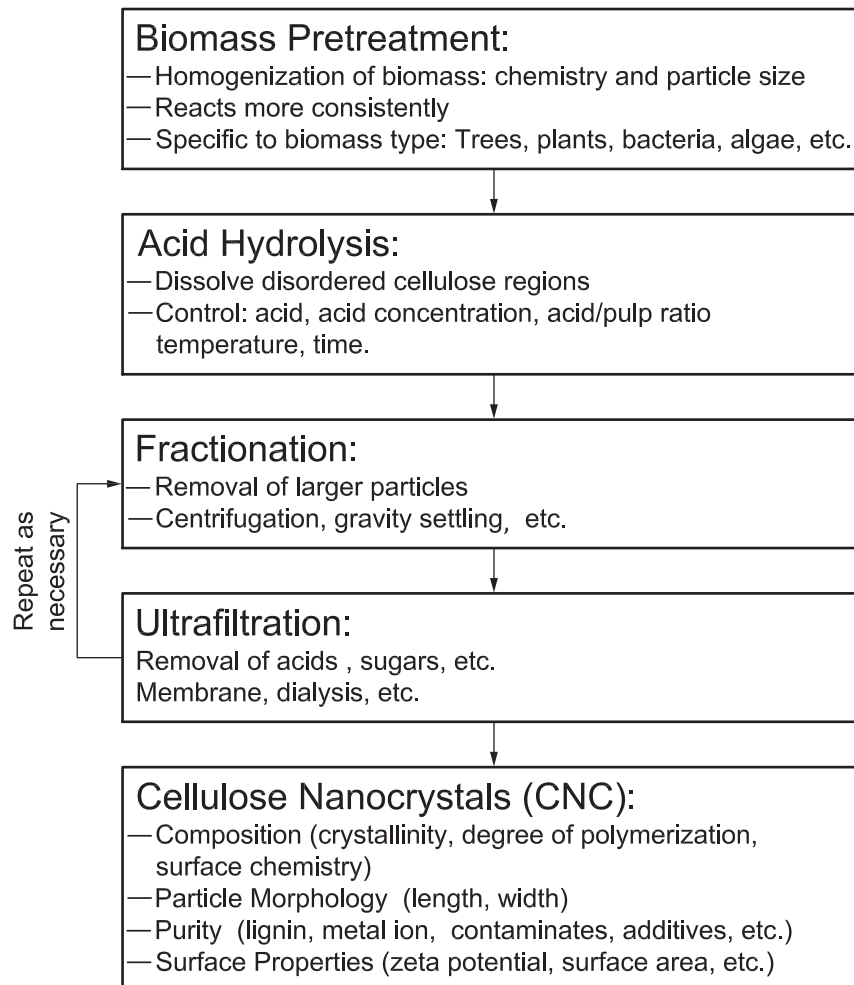


**Figure 2 — Overview of a typical process for production of CNCs by acid hydrolysis**

CNCs produced by sulfuric acid hydrolysis have negatively-charged sulfate half-esters on their surface which result in stable aqueous colloidal suspensions. Negatively charged CNCs are also formed by phosphoric acid hydrolysis, whereas hydrochloric acid gives uncharged CNCs with only surface hydroxyl groups. Oxidation catalysed by TEMPO (2,2,6,6-tetramethyl-1-piperidinyloxy free radical) can be used to convert surface hydroxyls to carboxylic acids for CNCs generated using either sulfuric or hydrochloric acid.[19][20] Oxidation with ammonium persulfate also generates carboxylated CNCs.[16] The CNC dimensions vary with the source of the cellulose; CNCs derived from wood pulps typically have average lengths of 100 nm to 200 nm and cross-sections of 4 nm to 9 nm, whereas those from bacterial and tunicate sources can be considerably larger, with lengths of 1  $\mu\text{m}$  to 2  $\mu\text{m}$  and cross-sections up to 50 nm (as reviewed in Reference [2]). The preparation method, acid or oxidant concentration, reaction time and temperature, and sonication steps during purification also affect the CNC dimensions and the overall yield and kinetics.[21][22][23][24][25][26][27]

The acidic CNC suspensions produced by acid hydrolysis can be used in never-dried form. However, in most cases the proton can be replaced by other cations by neutralizing the CNC suspension with aqueous bases, such as hydroxides (XOH) or carbonates ( $\text{X}_2\text{CO}_3$ ), to give a salt form of the CNCs (X-CNC, where X is the *counterion* associated with the anionic group). The pH-neutral sodium form, Na-CNC, is most typically produced commercially and at large scale by in-line neutralization of H-CNCs with sodium hydroxide (NaOH) or sodium carbonate ( $\text{Na}_2\text{CO}_3$ ). Advantages, such as the water-dispersability of the dried product,[28] allowing spray-dried or freeze-dried CNCs to be stored and shipped in the dry form at significantly lower cost and then re-suspended at the point of use, account for this preference. Proton counterions are most often exchanged for others by neutralization of the acidic groups with

aqueous hydroxide bases,<sup>[29]</sup> but this can also be accomplished by treatment with the appropriate ion-exchange resin.<sup>[30]</sup>

Dry CNC samples are prepared from the initial aqueous suspensions by evaporation, oven-drying, freeze-drying (lyophilization), or spray-drying. Some characterization methods require dry samples, whereas others employ a dilute suspension of CNCs. If the CNCs are already available as an aqueous suspension, the sample can be diluted to the required concentration using deionized water or dilute buffer or salt (NaCl) solution. Dry samples can be redispersed in pure water; general guidelines for dispersion of powders in liquids can be found in ISO 14887<sup>[31]</sup>. Although an ultrasonic treatment step is typically used to break up aggregates and agglomerates, a lack of reproducibility might contribute to variability of results, as summarized in a recent study aimed at standardizing procedures for ultrasonic dispersion of nanoparticles.<sup>[32]</sup> It is not trivial to obtain redispersed samples of CNCs that have size distributions and levels of aggregates or agglomerates that are similar to those of a purified, but never-dried, sample. An early study showed that films of CNCs with fully protonated sulfate half-esters could not be redispersed after drying, whereas CNCs with monovalent cations, such as sodium were redispersed with mild ultrasonic treatment to give stable colloidal suspensions that were similar to those prior to drying.<sup>[29]</sup> Detailed procedures for the redispersion of the neutral sodium-form of CNCs prepared by evaporation, lyophilization or spray-drying have been reported.<sup>[28]</sup> The counterion and moisture content of the dry CNCs and the sonication conditions (energy, CNC concentration) were all shown to affect the CNC (re) dispersibility. While the sodium-form CNCs were fully dispersible when completely dried, the protonated CNCs were only fully dispersible above a threshold water content of 4 wt %.

In this Technical Report, emphasis is placed on CNCs manufactured using sulfuric acid, with sulfate half-ester groups on the cellulose surface (cellulose sulfate); unless otherwise noted, all examples are for this form of CNCs. This reflects the emphasis on this material, in both commercial and research laboratories. Most of the characterization methods are also applicable, in some cases with appropriate adjustments, to other chemical forms of CNCs or cellulose nanofibres. For example, the detection and quantification of surface functional groups is specific to the specific CNC production method. The nature of the CNC counterion is important for some measurands, notably determination of the surface charge due to sulfate half-ester or carboxylate groups by conductometric titration (see 5.2.1 and 5.2.2) and zeta potential (see 7.2). Unless otherwise mentioned, the particular counterion in the CNC sample does not affect the characterization methods discussed in this Technical Report.

Cellulose nanocrystals have specific physico-chemical properties associated with both the underlying cellulose particle and the surface chemistry imposed by its manufacturing process. At the point of commercialization, it is necessary to clarify the several descriptive systems that have been used in this field: the geometric forms in nanotechnology, the industrial production method, and the chemical form used in national regulations. All three are found in the recent approval under Canada's New Substances Notification Regulations<sup>[33]</sup> as it provides the following:

- a) chemical description (cellulose, hydrogen sulfate, sodium salt with a total sulfur content greater than or equal to 0,5 % and less than or equal to 1,0 % by weight);
- b) production method description (obtained from sulfuric acid hydrolysis of bleached pulp);
- c) geometric description of length (nominal length of 100 nm  $\pm$  50 nm) and cross-section (cross-sectional dimensions of less than or equal to 10 nm). As suggested in ISO 12805, composition, length, diameter and surface area are the critical parameters to be considered first in setting specifications.<sup>[34]</sup>

## 5 Composition

### 5.1 Chemical composition

The chemical identity of CNCs as cellulose can be assessed by a qualitative identification test employed for microcrystalline cellulose; dispersion of dry CNCs in iodinated zinc chloride will result in a violet-blue colour.<sup>[35]</sup> Their composition can also be verified by elemental analysis, based on the formula  $[(C_6H_{10}O_5)_n]$  and taking into account surface functional groups if their degree of substitution is known.

Although elemental analysis provides some information on surface functionality (e.g. % S for sulfate half-esters), more detailed tests are typically used to quantify surface functional groups (see 5.2). The identity of inorganic metal counterions for CNCs with anionic surface groups can be determined by inductively coupled plasma-optical emission spectroscopy (ICP-OES) using the procedure outlined in 5.4.1 for sulfur. The density of CNCs has usually been assumed to be the same as other types of cellulose,<sup>[2]</sup> as confirmed by a recent determination of 1,56 g/cm<sup>3</sup> and 1,63 g/cm<sup>3</sup> for the densities of sulfated and unsulfated CNCs.<sup>[36]</sup>

## 5.2 Surface functional groups

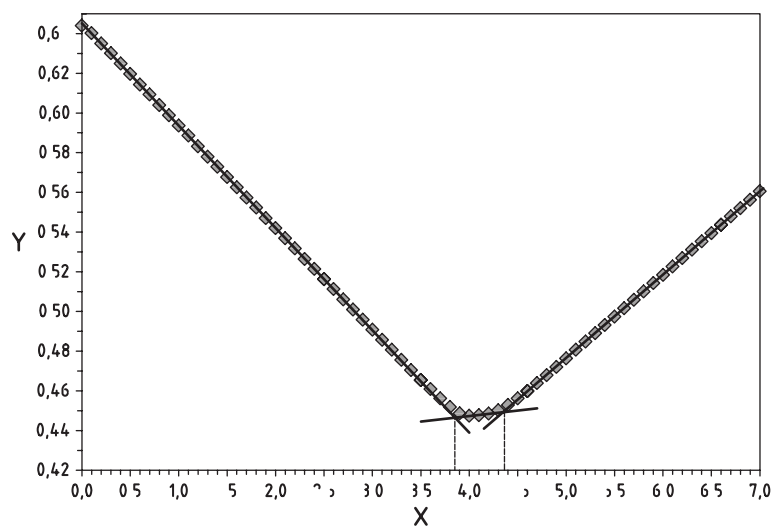
### 5.2.1 Determination of sulfate half-esters

CNCs extracted by sulfuric acid hydrolysis have sulfate half-ester groups on their surface. The concentration of these negatively charged groups determines the CNC surface charge density and controls the colloidal stability of CNCs in aqueous suspension, along with the self-assembly behaviour and rheological properties. Two approaches have been used to determine the sulfate half-ester content. The first relies on measurement of total sulfur content by elemental analysis.<sup>[26][27]</sup> In cases where the sample has been purified to ensure removal of all residual unbound sulfate ions, the total sulfur content can be converted directly to the CNC sulfate half-ester content.<sup>[37]</sup> The second approach uses conductometric titration of the acidic sulfate half-ester groups on the CNC surface using an aqueous base. Both methods are described in this Clause, followed by a comparison of results for various CNCs.

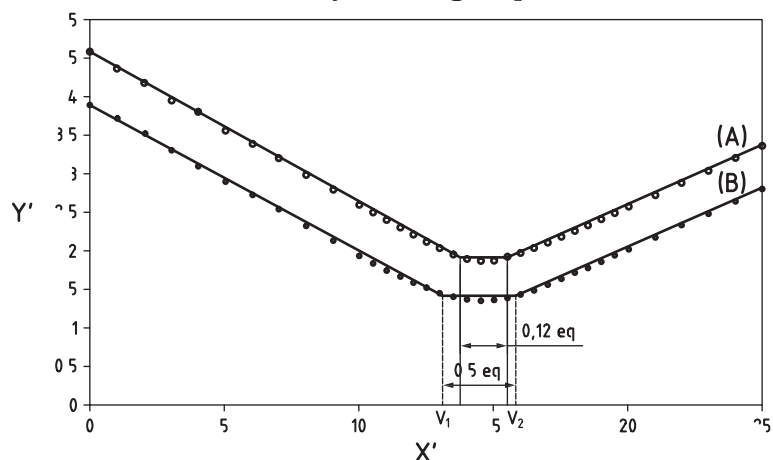
Measurement of the total sulfur content can be accomplished by elemental analysis or by ICP-OES using a spectrometer equipped with a concentric nebulizer, a cyclonic spray chamber and a quartz torch with a quartz injector tube, optimized according to the manufacturer's specifications. The sample is completely solubilized by microwave assisted sample digestion using high purity nitric and hydrochloric acids in high pressure closed vessels or, by wet ashing with strong acids, such as nitric and perchloric.<sup>[38]</sup> A block digestion system can be used to evaporate excess acids after the initial digestion. Analyses are conducted by ICP-OES using the sulfur emission lines at 180,669 nm and 181,972 nm. Calibration is accomplished by the method of additions (to compensate for any residual matrix interferences) in which incremental spikes of sulfur as sulfate are prepared from a standard sulfur solution (e.g. a primary standard, such as NIST SRM 3154). Samples can be diluted to ensure linearity of response. Samples are gravimetrically spiked with at least two incremental levels of appropriate amounts of known calibration standard. The levels should be chosen such that the spike results in a one to twofold increase in the total sulfur concentration in the sample with each spike and the analytical response is linear. The calculation of the concentration of sulfur requires a three point (minimum) standard additions calibration. Since the slope of the standard additions calibration function for the sample and blank are likely not equivalent, separate calibrations for  $C_s$  and  $C_{blk}$  should be performed. Note that although total sulfur content can also be obtained by inductively coupled plasma mass spectrometry (ICP-MS, see 5.6.3) ICP-OES is the more reliable and straightforward method unless the sulfur concentration is very low.

The sulfate half-ester content can be determined by conductometric titration of the acidic sulfate half-ester groups on the CNC surface using an aqueous base, such as sodium hydroxide.<sup>[30][39]</sup> This is the most commonly used method for this purpose.<sup>[40]</sup> The sample should first be purified by extensive dialysis to remove any residual ions and then treated with H-form strong acid cation-exchange resin to ensure fully protonated sulfate half-esters. Commonly, CNC samples are diluted or re-dispersed with deionized water (typically to  $\leq 1,5$  wt %) and dialyzed against pure water until the pH and conductivity of the water surrounding the membranes no longer changes and approaches that of pure water. Hollow-fibre membrane dialysis systems can also be used, they reduce dialysis time by drastically increasing the exchange surface area and maintaining a large concentration gradient via counter-current sample and dialysate flow. Prior to CNC protonation, the H-form strong acid cation-exchange resin should be rinsed with a large excess of pure water until the filtrate is colourless and identical in pH and conductivity to the wash water. A large excess of resin should be added to dialyzed CNC suspension at a sufficiently low CNC concentration to ensure no coagulation, and the sample shaken to ensure uniform mixing. The resin is then removed by filtration. Multiple successive treatments with fresh resin might be required to achieve full protonation, particularly if the CNCs are in neutral salt form. Alternatively, passing the diluted suspension through a column filled with such resin results in faster treatment.<sup>[37]</sup> Such treatment ensures complete protonation of a pure CNC suspension containing

no residual dissolved ions, yielding a 1:1 ratio of sulfate half-esters to protons and ensuring accurate titration results. The concentration of the final protonated CNC sample is determined gravimetrically, a sample of known volume is weighed and placed in a beaker with a dilute salt (NaCl) solution and titrated against dilute sodium hydroxide using titration conditions optimized from the literature.<sup>[30]</sup> <sup>[41]</sup> The sample conductivity is measured once the sample has equilibrated after the addition of each aliquot of NaOH. Equivalence points are determined from the intersection of the regression lines fit to the data points in the distinct regions of the titration curve ([Figure 3](#)).



a) H-CNCs containing strong acid sulfate half-ester groups and a small quantity of weak acid carboxylic acid groups



b) TEMPO-oxidized CNCs generated with two different concentrations of oxidant

#### Key

X	volume NaOH added (ml)
Y	conductivity ( $\mu\text{S}/\text{cm}$ )
X'	volume NaOH (ml)
Y'	conductivity ( $\text{mS}/\text{cm}$ )

SOURCE Beck et al. 2014 and Habibi et al. 2006.[37][42]

**Figure 3 — Schematic illustration of conductometric titration curves**

When interpreting conductometric titration data, it is important not to confuse the protons that are actually detected (by neutralization with sodium hydroxide) with the sulfate half-ester content that is calculated from the titration results. The calculations are based on the assumption that the protons in the sample are in a 1:1 ratio with the sulfate half-ester groups. Despite this caveat, the titration method does not require specialized and expensive equipment, and can be very useful for quality control during CNC production.

Typical sulfate half-ester and sulfur content values for wood-based and other CNCs measured by titration and elemental analysis are shown in [Table 1](#). The differences between values obtained by these two approaches have been discussed in the literature for CNCs of varying degrees of protonation.

[30][37][39][43][44] Titration values are often lower than those found by elemental analysis;[40] this is primarily due to insufficient sample preparation of the CNCs analysed by titration, notably failure to ensure that the CNCs are fully protonated following purification by dialysis. Sodium-form CNCs are an extreme example for which the sulfate half-ester content would not be measurable by conductometric titration but would be by elemental analysis, such as ICP-OES. Treatment with mixed bed ion-exchange resin (which contains hydroxide form anion exchange resin) has also been found to remove elemental sulfur from CNC samples, and as such it is recommended to completely avoid the use of mixed bed ion-exchange in CNC suspension purification; only dialysis should be used.[37] Alternatively, the presence of contamination in the form of sulfur-containing species, such as sulfate ions will yield erroneously high elemental analysis (and conductometric titration, if they are protonated) results. This illustrates the importance of dialysis for CNC suspension purification.

Differences between sulfate half-ester/sulfur contents measured by titration and elemental analysis methods, respectively, might also be caused by the presence of sulfate half-ester groups that are inaccessible to titrant[39] or other forms of sulfur, introduced during biosynthesis of the source cellulose.[45] Owing to these discrepancies, if elemental analysis is used to estimate CNC surface charge from sulfate half-esters, it is recommended to perform concurrent elemental analysis of the cellulose source of the CNCs being studied to obtain an estimate of sulfur. It is important to understand that total sulfur (measured by elemental analysis methods, such as ICP), titratable sulfur (protonated sulfate half-ester groups that are accessible to titrant), sulfate half-ester content contributing to surface charge (all surface sulfate half-ester groups) and total sulfate half-ester content (sulfate half-ester groups that are titrant-accessible and -inaccessible, if any) are not necessarily equivalent values. However, a recent study has shown that total sulfur and titratable sulfur are equivalent for softwood kraft pulp-derived CNCs, indicating that all sulfate half-esters are at the surface.[37] In general, elemental analysis of the source cellulose and CNCs combined with conductometric titration of protonated CNCs will give the most complete picture. Elemental analysis of CNCs extracted from the same source by HCl hydrolysis might also be helpful in determining the “base sulfur content” of the CNCs. The above recommendations are particularly important if knowledge of the precise quantitative surface charge or sulfur content is required. Sulfur contents determined by the different methods typically vary by no more than around 0,1 wt %, provided the CNCs contain no sulfur-containing impurities and are fully protonated if required.[37]

An additional complication in assessing sulfate half-ester content arises for samples that have been extracted by sulfuric acid hydrolysis and then subjected to TEMPO-catalysed oxidation to generate surface carboxylic acids. It is difficult to measure sulfate half-ester (strong acid) content by conductometric titration if significant levels of weakly acidic carboxylic acids are present, but sulfate half-esters can be determined in the presence of low quantities of carboxylic acid groups as shown in [Figure 3 a](#)) for a non-oxidized CNC sample with a small number of weak carboxylic acid groups.[39][43]

Finally, the surface sulfur content has also been measured by X-ray photoelectron spectroscopy (XPS). [20][40][46][47][48][49] Values typically range between 0,3 to 0,6 atomic % S, although in a few cases the sulfur content was reported to be too low to be detected. In several examples, the surface sulfur content has been compared to conductometric titration results for CNCs with sulfur content similar to the data in [Table 1](#). [20][40][48] In one study, both methods showed lower sulfur content for desulfated CNCs than for the initial CNCs obtained by sulfuric acid hydrolysis.[40] However, quantitative agreement was poor, with the sulfur content showing a sixfold change by titration but only a twofold change by XPS. Although the film thickness was not reported, one should in principle obtain the same sulfur content for the two methods when films of a single monolayer of CNCs are measured by XPS, since the depth penetration of ~10 nm is greater than the particle cross-section (see [5.6.4](#) for more details on XPS measurements of CNCs).



**Table 1 — Sulfate half-ester and sulfur contents (in mmol/kg CNC) for various CNC samples**

Cellulose source	Titration (standard deviation) <sup>a</sup>	Elemental analysis (standard deviation) <sup>a</sup>	Pre-treatment	Reference
Cotton	205 (10)	220 (20) <sup>b</sup>	Dialysis, mixed bed ion-exchange resin	[44]
Softwood (bleached kraft pulp)	84	240 <sup>c</sup>	Dialysis	[39]
Bacteria (Nata de coco)	5	—	Dialysis	[19]
Hardwood (eucalyptus)	250	—	Dialysis, mixed bed ion-exchange resin	[21]
Softwood (bleached sulfite pulp)	290 (35)	—	Dialysis, mixed bed ion-exchange resin	[21]
Softwood (dissolving-grade sulfite pulp)	293	0,57 atom % <sup>d</sup>	Dialysis	[40]
Cotton	221 (6)	193 <sup>e</sup>	Dialysis, strong acid cation-exchange resin	[30]
Cotton	181 (6)	193 <sup>e</sup>	Dialysis, mixed bed ion-exchange resin	[30]
Softwood (bleached kraft pulp)	225 (15)	225 (15) <sup>f</sup>	Dialysis, strong acid cation-exchange resin	[37]
<p><sup>a</sup> Standard deviation is listed when it was provided in the literature reference.</p> <p><sup>b</sup> Elemental analysis technique not specified.</p> <p><sup>c</sup> Elemental analysis by X-ray fluorescence analysis.</p> <p><sup>d</sup> Elemental analysis by XPS (based on C, O and S content).</p> <p><sup>e</sup> Elemental analysis by quantitative conversion of sulfur to SO<sub>2</sub> by combustion. The analyser uses IR or thermal conductivity to detect sulfur in the combustion gases.</p> <p><sup>f</sup> Elemental analysis by ICP-OES (total sulfur).</p>				

### 5.2.2 Determination of carboxylic acids

The carboxylate content of oxidized CNCs can be determined by conductometric titration with sodium hydroxide using a similar approach to that described in 5.2.1. Typically, a known amount of a strong acid, such as hydrochloric acid (HCl) is added prior to titration, ensuring full protonation of the weak carboxylic acid groups.[41][50][51] The carboxylate content is determined by extrapolating and intersecting the three linear portions of the curve (strong acid, weak acid, excess titrant) to give the two equivalence points (strong acid and total acid). Subtracting the strong acid content from the total acid content gives the weak acid (carboxylate) content [Figure 3 b)]. As described in 5.4.1, the presence of strong acid sulfate half-ester groups hinders the determination of carboxylic acid content by conductometric titration in sulfated CNCs that have been highly oxidized (e.g. by TEMPO-mediated oxidation).

Determination of surface carboxylic acids by conductometric titration has typically been reported as degree of oxidation, which is defined as the mass fraction of carboxyl groups in the CNC sample.[51] In several cases, the degree of oxidation has been measured as a function of the oxidant/cellulose ratio for TEMPO-catalysed oxidation; a plateau value is obtained that is hypothesized to represent complete conversion of accessible surface hydroxyl groups to carboxylic acids.[19][42] Reported degrees of oxidation between 0,1 and 0,2 are typical;[16][42][50][52] in two cases the degree of oxidation corresponds to ~900 mmol/kg,[19][50] which is considerably higher than the typical values of 200 mmol/kg for sulfate half-esters (Table 1). Note that complete oxidation of surface hydroxyl groups will give different degrees of oxidation for CNC particles with different surface area/mass ratios. In cases where the fraction of surface, cellulose chains has been estimated based on the unit cell parameters for individual crystallites, the predicted degree of oxidation is similar to that obtained experimentally.[42][52]

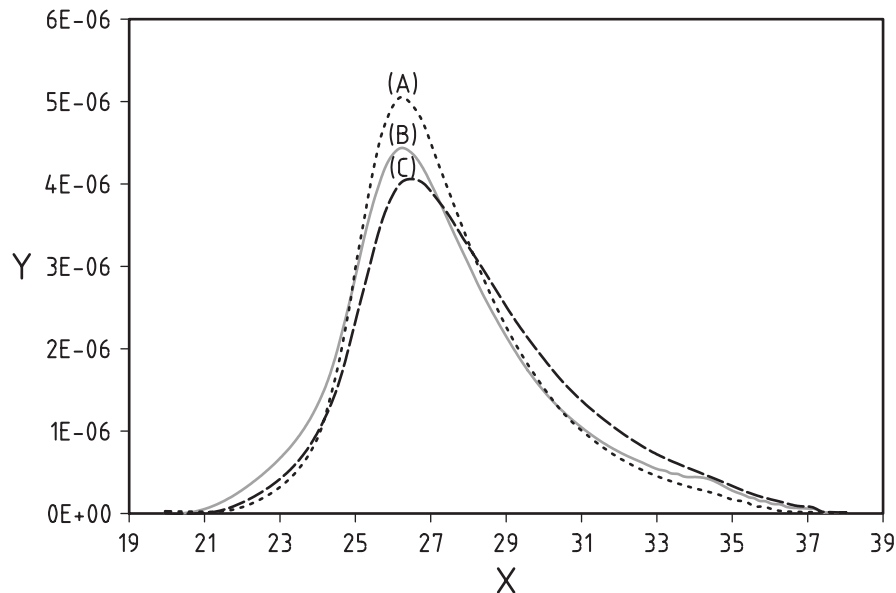
Carboxylic acid groups have also been quantified by Fourier transform infrared spectroscopy (FTIR) using the strong absorption band due to the carbonyl stretch of the carboxylic acid at  $1\,634\text{ cm}^{-1}$ .<sup>[20]</sup><sup>[42]</sup><sup>[51]</sup><sup>[52]</sup> The degree of oxidation is calculated as the ratio of the intensity of the  $1\,634\text{ cm}^{-1}$  band to that of strongest cellulose backbone band at  $1\,050\text{ cm}^{-1}$ . Note that use of the carbonyl stretch of the carboxylate anion at  $1\,608\text{ cm}^{-1}$  should be avoided due to interference from adsorbed water in this region.<sup>[51]</sup> In several cases, the FTIR method was shown to be in reasonable agreement with the results from conductometric titration,<sup>[20]</sup><sup>[42]</sup><sup>[52]</sup> although it has been concluded that the titration method is the more reliable and reproducible.<sup>[51]</sup>

### 5.3 Degree of polymerization

The degree of polymerization (DP) is the number of glucose units in individual cellulose polymer chains and provides a measure of the extent of cellulose degradation during CNC production. Acid hydrolysis of celluloses typically produces a rapid decrease in DP to a limiting or level-off value,<sup>[27]</sup><sup>[53]</sup> leading to the suggestion that the limiting DP is correlated with the size of individual crystals aligned along the long axis of the fibres prior to removal of amorphous cellulose.<sup>[8]</sup><sup>[53]</sup> This hypothesis has been confirmed in several studies as summarized in a recent review.<sup>[8]</sup> DP has been used to characterize CNC properties as a function of hydrolysis or oxidation conditions in a number of studies.<sup>[8]</sup><sup>[27]</sup><sup>[51]</sup><sup>[54]</sup><sup>[55]</sup><sup>[56]</sup><sup>[57]</sup><sup>[58]</sup> The limiting DP values depend on the cellulose source, with values ranging from 90 to 200 for wood pulp-derived CNCs and up to 6 000 for the larger CNCs isolated from algae.<sup>[8]</sup>

Two methods have been employed to measure DP for a variety of cellulosic materials, including CNCs. The first and simpler method relies on measuring the limiting (intrinsic) viscosity of cellulose dissolved in a solution of cupriethylenediamine, for which standard methods for pulps (ISO 5351<sup>[59]</sup>), cellulose (ASTM D1795-13<sup>[60]</sup>) and paper and board (ASTM D4243-09<sup>[61]</sup>) are available. These International Standards note that the presence of lignin might interfere with the viscosity determination, although this is likely to be less of an issue for CNCs compared to other cellulosic materials. The ISO and ASTM standards have slightly different expressions for calculating the limiting viscosity. Several expressions have been used to relate the limiting viscosity to the average DP, as summarized in ISO 5351:2010, Annex C. An investigation in which DP values were used as one parameter to optimize the hydrolysis conditions for CNC extraction from chemical pulps determined that two different methods for calculating DPs led to the same general conclusions.<sup>[27]</sup>

The second method for measuring DP of cellulosic nanomaterials is size exclusion chromatography (SEC) using either standard samples for calibration purposes or direct size determination by multi-angle light scattering. The SEC method has the advantage of providing a DP distribution, rather than an average DP value (Figure 4). This method requires that the cellulose be completely dissolved prior to chromatographic analysis, which has been accomplished by dissolving in metal-containing solvents, such as N,N-dimethylacetamide with lithium chloride, which disrupt the hydrogen bonding networks that prevent solubility in common solvents or by chemical modification to give a solvent-soluble cellulose derivative.<sup>[55]</sup><sup>[62]</sup> The various approaches for chemical modification have been critically reviewed, leading to the conclusion that the conversion of free hydroxyl groups to carbanilates using phenyl isocyanate in dimethyl sulfoxide is the preferred method.<sup>[55]</sup> Calculation of the DP distribution by SEC requires the complete conversion of hydroxyls to carbanilates, the choice of solvent was shown to have a significant impact on conversion, particularly for lignin or hemicellulose containing pulps. Despite the advantages of SEC for determining DP distributions, this method has been less widely used than the simpler viscosity method for CNCs.<sup>[56]</sup><sup>[58]</sup>



### Key

X elution volume (ml)  
Y relative concentration

SOURCE Kloser and Gray 2010.[58]

**Figure 4 — Size exclusion chromatography plots used to determine the degree of polymerization for sulfated (B), desulfated (C), and polymer modified (A) CNCs**

## 5.4 Crystallinity

### 5.4.1 General

The assembly of individual cellulose chains to give elementary fibrils that pack into larger units leads to regions of highly ordered (crystalline) cellulose as well as disordered (amorphous) regions. The crystalline fraction depends on the cellulose source, the initial enzymatic biosynthesis and changes induced by the extraction process.[2] CNC crystallinity is an important parameter to assess, since it affects the physical, chemical and mechanical properties of CNCs and composite materials in which they are incorporated. There are several crystalline forms of cellulose, of which cellulose I is the form that is naturally produced by a variety of organisms. Cellulose I exists as a mixture of two polymorphs (allomorphs) which vary in relative amounts depending on the cellulose source. Cellulose I<sub>α</sub> has a triclinic structure and predominates in algae and bacteria, whereas the monoclinic cellulose I<sub>β</sub> is the most abundant polymorph in higher plants and tunicates. The fraction of crystalline cellulose in a variety of cellulosic materials, including CNCs, has been studied extensively by X-ray diffraction (XRD) and more recently by complementary methods, such as solid state <sup>13</sup>C nuclear magnetic resonance (NMR) and infrared (IR) and Raman spectroscopies.[63][64][65][66][67][68] The various methods provide information on the fraction of the two crystalline polymorphs, the crystallinity (defined as the mass fraction of the sample comprised of crystallites) and in the case of XRD, the size of the individual crystallites. As noted in recent reviews,[63][64] the estimated crystallinity for cellulosic materials varies significantly depending on the choice of measurement and analysis method. This variation partly reflects the fact that different methods measure different properties. Furthermore, data analysis requires measuring peak heights or peak areas, frequently for overlapping peaks that require correction for background signals, and a variety of different deconvolution and data analysis methods have been employed. Additionally, in some methods (XRD), the crystallinity depends on the instrument used. The general approaches used for determination of the % crystallinity by XRD, NMR and vibrational spectroscopy are discussed below, followed by a comparison of results obtained for CNCs. Note that most of the

method development in this area has focused on wood pulps or larger cellulose fibrils, rather than CNCs. Although various terms have been used to describe the degree of cellulose order/disorder in the literature, we have used primarily the terms disordered and crystalline (% crystallinity) in this clause.

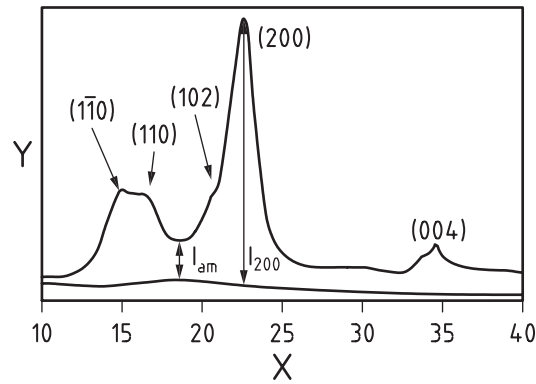
#### 5.4.2 X-ray diffraction

Cellulosic nanomaterials give a characteristic diffraction pattern with contributions from both crystalline and disordered components [Figure 5 a), b) and c)]. The % crystallinity can be assessed from the relative intensities of each component and the various methods to do so have been reviewed recently. [63][64][69] The simplest and most widely used method was developed in the 1950s by Segal[70] and is based on the peak height of signals at  $2\theta$  diffraction angles of  $22,8^\circ$  and  $18^\circ$ , representing crystalline and disordered cellulose, respectively. This peak height method [Figure 5 a)] estimates the crystallinity index [CrI (or CI), defined as the mass fraction of the sample comprised of crystalline cellulose] from the heights of the crystalline ( $I_{200}$ ) and disordered (amorphous,  $I_{AM}$ ) peaks, after correction for the background intensity, Formula (1).

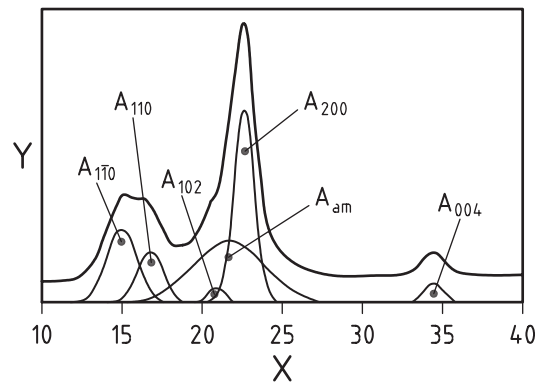
$$\text{CrI} = (I_{200} - I_{AM}) / (I_{200}) \times 100 \quad (1)$$

This method does not account adequately for the actual position of the broad amorphous peak and uses data for only one of the several crystalline peaks. Furthermore, the peaks due to crystalline and disordered cellulose vary in width. It is generally accepted that this empirical peak height method overestimates the % crystallinity.[64]

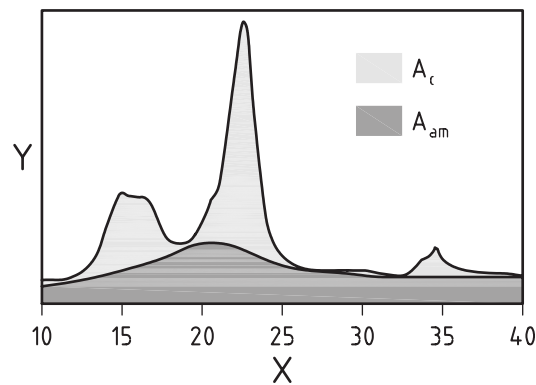
A second, more rigorous approach employs a deconvolution routine to separate the disordered and crystalline contributions to the diffraction spectrum [Figure 5 b)]. This curve fitting procedure requires information about the shape and number of crystalline peaks and makes the assumption that peak broadening is due to the amorphous cellulose content, ignoring any possible contributions from the crystallite size. After deconvolution of the spectrum, the crystallinity is calculated as the ratio of the area of all crystalline peaks to the total area. A third approach [Figure 5 c)] [64][71] determines the crystallinity by subtracting the disordered contribution from the diffraction spectrum. The disordered contribution is measured separately using a completely disordered sample.



a) Peak height method



b) Peak deconvolution method



c) Amorphous subtraction method

**Key**X  $2\theta$ 

Y intensity

SOURCE Park et al., 2010[64] and Moon et al., 2014.[68]

**Figure 5 — X-ray diffraction spectra for cellulose (Avicel PH-101) illustrating three methods for calculating the crystallinity index**

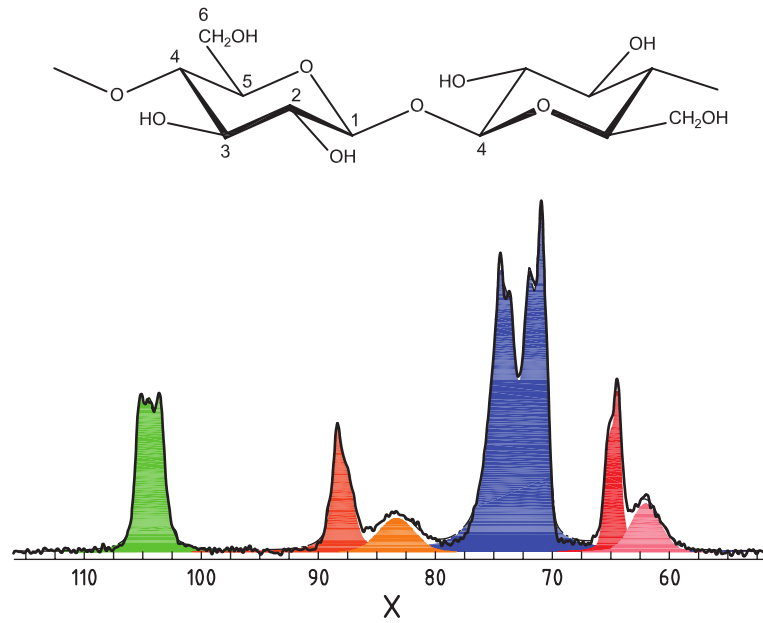
The crystallite size can be estimated from XRD measurements using the Scherrer formula,<sup>[72]</sup> which relies on measurement of the half-width of the crystalline peak and assumes that the peak broadening is dominated by the finite size of the crystallites.<sup>[72]</sup> The estimated broadening should be considered a lower limit as instrumental broadening and crystal lattice defects might also contribute to the line broadening.<sup>[63][73]</sup> Although the peaks for  $I_{\alpha}$  and  $I_{\beta}$  cellulose occur at slightly different diffraction angles, they are broad and are not typically used to quantify the ratio of the two polymorphs.<sup>[74]</sup>

### 5.4.3 Nuclear magnetic resonance

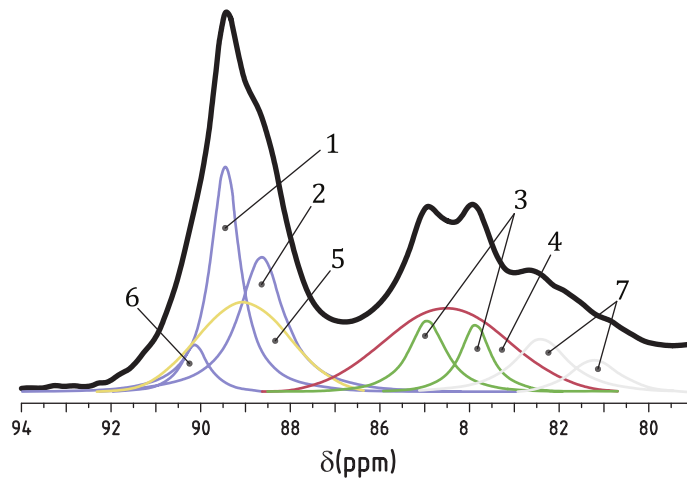
Cross polarization magic angle spinning (CP-MAS) solid state  $^{13}\text{C}$  NMR has been used to estimate the crystallinity for cellulose nanomaterials, including CNCs,<sup>[64][75][76]</sup> although much less frequently than XRD. The cellulose carbon signals occur between 55 ppm and 120 ppm [see [Figure 6 a\)](#)] with broad, but well-separated, peaks assigned to C1, C4 and C6 carbons. The C4 carbons have distinct resonances due to crystalline carbons at ~85 ppm to 92 ppm and disordered carbons at ~80 ppm to 85 ppm. The C6 carbons also show separate peaks due to crystalline and disordered cellulose. The most common approach for estimating crystallinity takes advantage of this difference in chemical shift and uses the total integrated intensities under the C4 crystalline and disordered peaks to calculate the crystallinity.<sup>[64][65]</sup> For example, a crystallinity of 64 % is measured from the intensities of the amorphous and crystalline signals for the C4 and C6 carbons for the spectrum shown in [Figure 6 a\)](#) for wood-pulp CNCs produced by sulfuric acid hydrolysis. Extensive NMR studies of various types of cellulose have employed a variety of peak fitting and deconvolution approaches to analyse the spectra in more detail. As an example, the signal due to crystalline C4 carbon can in some cases be separated into components arising from both  $I_{\alpha}$  and  $I_{\beta}$  polymorphs and from para-crystalline cellulose [see spectrum of C4 region after deconvolution in [Figure 6 b\)](#)]. Para-crystalline cellulose is less ordered than the crystalline component but more ordered than the disordered cellulose and is generally assigned to cellulose chains directly below the surface of the cellulose fibre or distortions in the interior. C1 and C6 carbons are also useful for quantifying the ratio of  $I_{\alpha}$  and  $I_{\beta}$  polymorphs as they show a single resonance for  $I_{\alpha}$ -cellulose but a doublet for  $I_{\beta}$ .<sup>[77]</sup> Peak fitting and deconvolution approaches have been used to resolve the C4 carbon resonance for disordered cellulose into accessible and inaccessible carbons [[Figure 6 b\)](#)], which can provide an assessment of surface area, as discussed in [7.1](#). Detailed descriptions of these approaches and references to the primary literature can be found in several reviews.<sup>[65][77]</sup>

An alternate approach has been used to estimate cellulose crystallinity from CP-MAS  $^{13}\text{C}$  NMR data. This method relies on the differences in the proton rotating frame relaxation time constants ( $T_{1\rho}(\text{H})$ ) to resolve peaks due to ordered and disordered cellulose. The resonances due to noncrystalline cellulose decay more rapidly than those due to crystalline components, so that spectra recorded at two or more  $T_{1\rho}(\text{H})$  can be used to obtain the fraction of crystalline cellulose.<sup>[65][78]</sup>

A recent review has critically compared the XRD and NMR methods based on a survey of literature data from different laboratories for one commercial cellulose (Avicel PH-101) and estimation of the crystallinity for a selection of eight commercial celluloses using the methods described in [5.4.2](#) and this subclause.<sup>[64]</sup> This study concluded that the peak height XRD method gives values that are significantly higher than other methods and provides, at best, a rough approximation of the disordered content. The other methods provided a narrower range of crystallinity values but the authors concluded that it was not possible to identify which method provided the most accurate evaluation of the crystallinity. Furthermore, it is important to consider that NMR will include surface groups in the disordered fraction, so that crystallinities will be lower than those measured by XRD, which estimates the total volume fraction of crystalline cellulose.<sup>[79]</sup>









a) CNCs produced by sulfuric acid hydrolysis of wood pulps



b) Cellulose fibrils (C4 region only) where AFS and IAFS are accessible and inaccessible disordered surfaces

**Key**

X	<sup>13</sup> C chemical shift [ppm]	
	C2, 3, 5	1 I <sub>α</sub> + I <sub>β</sub>
	C1	2 I <sub>β</sub>
	C4, crystalline	3 AFS
	C4, amorphous	4 IAFS
	C6, crystalline	5 para-crystalline
	C6, amorphous	6 I <sub>α</sub>
		7 hemi-cellulose

SOURCE Idstrom et al. 2013.[\[80\]](#)

**Figure 6 — <sup>13</sup>C cross polarization magic angle spinning solid state NMR spectra**

#### 5.4.4 Vibrational spectroscopy

Vibrational spectroscopy has been used for both qualitative and quantitative assessment of crystallinity for cellulosic materials and has the potential to provide quicker results using less costly equipment (compared to XRD or NMR) for routine measurements. Early studies employed IR spectroscopy to provide qualitative predictions of crystallinity; the subsequent development of FTIR spectrometers enabled quantitative measurements. Several infrared approaches have been developed and are based on measuring ratios of peaks due to disordered and crystalline content, or measuring the intensity of peaks sensitive to crystalline content relative to a reference peak that does not vary with crystallinity.[81][82][83][84][85] An initial crystallinity index, also referred to as the lateral order index, used the intensity ratio for peaks at  $1\,429\text{ cm}^{-1}$  due to  $\text{CH}_2$  bending modes and  $893\text{ cm}^{-1}$  due to deformation of anomeric CH as a measure of crystalline and amorphous content, respectively.[86] An alternative approach, the (total) crystallinity index, was based on the intensity ratio for signals at  $1\,372\text{ cm}^{-1}$  and  $2\,900\text{ cm}^{-1}$  due to CH bending modes and CH and  $\text{CH}_2$  stretching modes, respectively. The intensity of the CH bending mode increased with crystalline content, whereas the CH stretch was unaffected by variations in crystallinity.[83] A similar approach using a  $1\,280\text{ cm}^{-1}$  CH bending band that varied with crystallinity and an OH bending band at  $1\,200\text{ cm}^{-1}$  has also been employed.[85] In most cases, the infrared methods were validated or calibrated by using test samples of known crystallinity or comparing the measured crystallinity to values obtained by X-ray diffraction. A final approach, the hydrogen bonding intensity, is an empirical relationship based on the intensity ratios for peaks at  $3\,336\text{ cm}^{-1}$  and  $1\,336\text{ cm}^{-1}$ , due to intramolecular hydrogen bonds and an OH stretch, respectively.[81][82] This relationship is related to the well-ordered crystalline phase and the degree of intermolecular regularity. Each of these approaches reports on a somewhat different aspect of sample crystallinity/disorder and it is generally concluded that FTIR provides only qualitative information on crystallinity.[63][64]

Raman spectroscopy has also been applied to measure cellulose I crystallinity. An initial method was based on quantifying changes in the methylene bending modes at  $1\,481\text{ cm}^{-1}$  (crystalline) and  $1\,462\text{ cm}^{-1}$  (disordered).[67] More recently, a detailed survey of spectra for crystalline and disordered cellulose compared results for univariate and multivariate Raman methods and concluded that the intensity ratio for bands at  $380\text{ cm}^{-1}$  and  $1\,096\text{ cm}^{-1}$  provides a more sensitive method for detecting changes in crystallinity.[66] This approach was subsequently validated for a number of different cellulose sources which had contributions from fluorescence background and from lignin and hemicelluloses; the Raman data were in good agreement with XRD crystallinities calculated using the peak height method with amorphous correction.[87] The  $380\text{ cm}^{-1}$  Raman method has recently been applied to estimate crystallinities of CNCs and CNFs.[88] In addition to crystallinity measurements, vibrational spectroscopy has been used to assess the ratio of cellulose  $I_\alpha$  and  $I_\beta$  polymorphs.[77][89]

#### 5.4.5 Crystallinity measurements for CNCs

In most cases crystallinity measurements using XRD, NMR, or vibrational spectroscopy require dry samples. Some sample preparation methods use the dry material directly, whereas in other cases thin film samples are prepared by depositing a suspension onto a suitable support and drying. For XRD, samples are prepared by pressing dry CNCs onto a clean silicon or glass disc or by compressing the powder into a disc, typically at  $100\text{ kPa}$ – $1\text{ GPa}$  pressure. Alternatively, a suspension of CNCs in water is deposited onto a silicon disc and allowed to dry. The sample preparation method can introduce orientation of the crystals which will influence the intensities of the diffraction peaks, so affecting both  $C_{rl}$  and crystallite size.[64] It has been recommended that reflection mode measurements and side-loaded samples be employed to minimize these effects.[69] For NMR samples of dry CNCs are placed in zirconium oxide MAS rotors with typical spinning rates between  $3\text{ kHz}$  and  $10\text{ kHz}$ . Rehydrated samples or never-dried suspensions that are concentrated to remove most of the water can also be measured by CP-MAS. For FTIR, dry CNCs are pressed into potassium bromide disks or suspensions are used to deposit a thin film on an attenuated total reflection crystal.

As summarized in a 2011 review,[2] plant-derived CNCs have reported crystallinities between  $54\%$  to  $88\%$ , whereas tunicate derived CNCs generally have values in excess of  $80\%$ . Table 2 summarizes recent data measured for CNCs by XRD and NMR. The data have been selected primarily from studies in which several complementary methods have been used to characterize CNCs, including crystallinity and morphology. In one case, CNC crystallinity was measured by XRD for wood pulp CNCs as a



function of acid concentration and hydrolysis time.[27] The peak height method gave higher values than the deconvolution (peak area) method, the same trend observed for other cellulosic materials. [27] Notably, the difference between the two methods was approximately twice as large for samples with low crystallinity (see first entry in Table 2). The crystallinity as measured by the deconvolution method varied between 68,9 % and 89,1 %, with the highest values (~90 %) and the smallest crystal sizes (~6 nm, cross-section) obtained with 64 % acid at 45 °C. As expected, the highest crystallinity corresponded to a minimum degree of polymerization. A similar trend of higher crystallinity (up to 90,7 %) for longer hydrolysis times was observed for CNCs extracted from rice straw.[90] Crystallinity values of close to 90 % were also measured for CNCs extracted from ramie and cotton.[91] Carboxylated CNCs produced by oxidation of cotton and wood pulp have reported crystallinity of 85 % and 83 %, close to the maximum values for CNCs extracted with sulfuric acid.[16][50] Note, however, that lower values are obtained in other cases (Table 2); comparisons between samples, laboratories and methods are difficult since changes in crystallinity might be offset by effects of sample preparation or data analysis.

Overall, the XRD data suggest that a limiting crystallinity ~90 % is achievable for plant-derived CNCs, as measured by XRD. By contrast, NMR studies have reported values of ~60 % for wood-based CNCs,[24][79][92][93] using either the C4 peak intensity method or the relaxation time method. Interestingly, one of these studies[79] found higher crystallinity for both bacterial and tunicate CNCs, consistent with earlier data.[2] As noted above, NMR will include surface sugars as part of the amorphous contribution; since small particles have a larger fraction of surface atoms than large particles, one might expect a larger discrepancy between XRD and NMR results for CNCs than for larger cellulose fibres.

There are few examples where multiple methods have been used for the same sample.[24][50][75][94] For a CNC reference material,[94] both deconvolution and peak height XRD methods were employed, with crystallinity ranging from 60 % to 90 %, but without a clear trend towards higher values for the peak height method. For the same sample, NMR gave a value of 64 %, based on the mean of data for both C4 and C6 resonances [Figure 6 a)]. In another comparison, NMR gave slightly higher values than XRD for wood-based CNCs.[24] Finally, the crystallinity of carboxylated CNCs (with either H<sup>+</sup> and Na<sup>+</sup> counterions) produced by ammonium persulfate oxidation of cotton was 85 %, compared to a lower value of 63 % for the lateral order index measured by FTIR in the same study.[50]

**Table 2 — Crystallinity and crystallite size for CNCs from various cellulose sources**

Cellulose source	Production method	Method (analysis) <sup>a</sup>	Crystallinity (%)	Crystallite size nm	Reference
Wood pulp	Sulfuric acid <sup>b</sup>	XRD (DC,PH)	68,9, 80,7	5,8 to 8,3	[27]
		XRD (DC,PH)	89,1, 84,6	—	[27]
Wood pulp	Sulfuric acid	XRD (DC)		3,4, 4,3, 4,5 <sup>c</sup>	[40]
	Hydrochloric acid	XRD (DC)		4,1, 4,2, 5,0 <sup>c</sup>	[40]
Wood pulp	Sulfuric acid	XRD (PH)	66,4	—	[49]
Sisal fibres	Sulfuric acid	XRD (PH)	81	4,5	[91]
Ramie	Sulfuric acid	XRD (PH)	88	5,3	[91]
Cotton	Sulfuric acid	XRD (PH)	88	6,0	[91]
Cotton	Sulfuric acid	XRD	—	4,5	[73]
Rice straw	Sulfuric acid	XRD (PH)	90,7	4,24	[90]
Bacterial	Sulfuric acid	XRD (DC)	85 <sup>d</sup>	—	[95]

<sup>a</sup> Analysis methods: For XRD DC = deconvolution and PH = peak height (see 5.4.2 for discussion of variability in crystallinity with measurement method and instrument and analysis procedures).

<sup>b</sup> Hydrolysis conditions: 25 min with 16 wt % acid, 45 °C (first line) and 65 wt %, 45 °C (second line).

<sup>c</sup> Dimensions of crystallites perpendicular to the three crystallographic planes.

<sup>d</sup> Similar values measured for sulfated and desulfated CNCs.

<sup>e</sup> A number of CNCs produced from other sources by ammonium persulfate oxidation were also studied.

Table 2 (continued)

Cellulose source	Production method	Method (analysis) <sup>a</sup>	Crystallinity (%)	Crystallite size nm	Reference
MCC	Sulfuric acid	NMR	~60		[92]
Wood pulp	Sulfuric acid	NMR	61–63	—	[24]
Wood pulp	Sulfuric acid	XRD	50–55	—	[24]
Wood pulp	Sulfuric acid	NMR	60	—	[79]
Bacterial	Sulfuric acid	NMR	72	—	[79]
Tunicate	Sulfuric acid	NMR	80	—	[79]
Cotton	Ammonium per-sulfate	XRD (PH)	85 (H <sup>+</sup> , Na <sup>+</sup> )	—	[50]
MCC, avicel <sup>e</sup>	Ammonium per-sulfate	XRD (DC)	82,7	—	[16]

<sup>a</sup> Analysis methods: For XRD DC = deconvolution and PH = peak height (see 5.4.2 for discussion of variability in crystallinity with measurement method and instrument and analysis procedures).

<sup>b</sup> Hydrolysis conditions: 25 min with 16 wt % acid, 45 °C (first line) and 65 wt %, 45 °C (second line).

<sup>c</sup> Dimensions of crystallites perpendicular to the three crystallographic planes.

<sup>d</sup> Similar values measured for sulfated and desulfated CNCs.

<sup>e</sup> A number of CNCs produced from other sources by ammonium persulfate oxidation were also studied.

## 5.5 Moisture content

The water content of CNC samples might be an important consideration for some applications. For example, some analytical tests require removing water from “dry” CNCs prior to analysis and the residual water content affects both the redispersibility of the sample [28] and its stability during storage. [96] When necessary, a quantitative determination of the water content can be obtained gravimetrically using standard methods developed for paper, pulp and boards, as outlined in ISO 638. [97] The procedure typically involves measuring the mass of a sample before and after oven drying (at approximately 105 °C); in cases where loss of other volatile components might also occur, the sample should be dried in a dessicator.

## 5.6 Contaminants

### 5.6.1 General

CNCs might in some cases contain trace amounts of other components that occur in the cellulosic biomass from which they are isolated. These include polysaccharides, such as hemicelluloses, amorphous cellulose that has not been completely removed during the production of CNCs, and in the case of plant-derived CNCs, lignin which forms a significant part of the plant cell wall. Contaminants are sometimes introduced during the isolation of CNCs (e.g. residual salts from the acid hydrolysis or oxidation that are not removed by dialysis, residual small molecules, such as fatty acids or terpenes). Residual metal ions might be present, either as impurities in the initial cellulosic biomass or introduced during the isolation of CNCs. It is important to note that these impurities, if detectable, are usually present in small amounts. Nevertheless, because even trace amounts of impurities can affect some CNC applications, information on typical procedures for their detection is provided in 5.6.2, 5.6.3 and 5.6.4. It should also be noted that additives which have been used to facilitate dispersion of CNCs might have to be quantified and/or removed.

### 5.6.2 Residual impurities derived from cellulosic biomass

Several standard methods are employed to quantify carbohydrate content and lignin content for pulp, paper and board samples. These methods can be readily adapted for use with CNC samples,<sup>[79]</sup> although in some cases the method detection limits might not be compatible with the trace amounts of the specific component in CNCs. For residual polysaccharides, the methods involve hydrolysis of the cellulose sample, followed by separation and quantitation of the individual monosaccharides by either gas-liquid chromatography (GLC)<sup>[98]</sup> or high-performance anion-exchange chromatography (AEC).<sup>[99]</sup> Standard samples of the various monosaccharides are required for calibration purposes. Lignin content in wood-based CNCs can be determined using a standard method that is applicable to lignin contents in the range of ~0,3 % to 3 % by weight.<sup>[100]</sup> Small molecules that are present in the initial cellulosic material and are not removed during CNC purification or organic species acquired during storage and handling of CNCs can be quantified using a solvent extraction method.<sup>[98][101]</sup> The method involves gravimetric determination based on the weight of the sample before and after Soxhlet extraction with solvents, such as dichloromethane, ethanol/benzene, or acetone. Note that dichloromethane will remove less polar compounds whereas ethanol (or acetone) removes low molecular weight sugars, phenols and other water-soluble materials.

### 5.6.3 Metal ions

Residual metal ions in CNCs pose a potential health and environmental risk and might interfere with other tests or some applications/end uses of the material. Quantitation of metal impurities can be undertaken by ICP-MS following complete solubilization of the sample by microwave-assisted mixed-acid digestion. Quantitation of Cr and Fe should be performed using a sector-field mass spectrometer in medium resolution mode ( $\Delta m/m \sim 4\ 000$ ) or a spectrometer equipped with a collision cell or dynamic reaction cell to eliminate potential interferences which arise from the other constituents of the sample or plasma. Microwave digestion of the sample and calibration by the method of standard additions are similar to the method used for total sulfur content by ICP-OES described in [5.2.1](#).

Although the standard additions method is frequently used for the determination of trace elements, significant signal drift can degrade the accuracy of the final results. The isotope dilution (ID) method with reverse ID calibration provides an alternative approach for applications that require enhanced measurement accuracy and precision.<sup>[102][103][104]</sup> ID is recognized as a primary method of measurement and is often used for the certification of reference materials.<sup>[102]</sup> This method permits accurate quantitation of analytes in samples once isotopic equilibration is achieved between the added spike and the endogenous analyte, compensating for loss of analyte during sample manipulation and suppression of ion sensitivities by elements present in the sample matrix. The ID method has been used to quantify the content of cadmium, chromium, copper, iron, mercury, nickel and lead in wood pulp CNCs.<sup>[94]</sup>

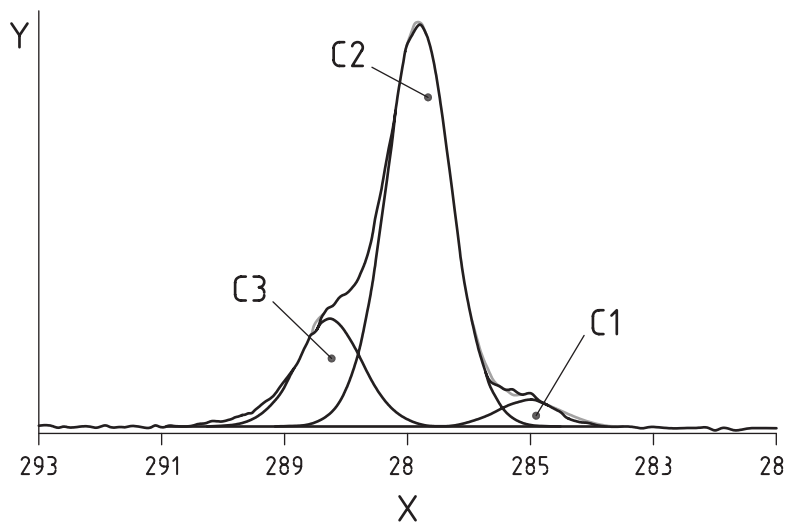
ICP-MS or ICP-OES can also be used to quantify the contamination of CNC samples with residual salts, such as sodium sulfate from their production by acid hydrolysis or oxidation. For example, the difference between the sodium and/or sulfur contents of a sample of Na-CNCs measured before and after extensive dialysis might give an indication of the amount of free salt present in the unpurified sample (see Reference [\[38\]](#)).

### 5.6.4 Detection of contaminants by X-ray photoelectron spectroscopy

X-ray photoelectron spectroscopy (XPS) has been employed in several studies for the detection of contaminants in CNCs<sup>[47][48][93][105][106]</sup> using the same methods that have been applied to other cellulosic materials.<sup>[107]</sup> XPS spectra are obtained by measuring the kinetic energy and number of electrons that escape from a surface that is irradiated with a beam of X-rays. Note that although XPS is a surface analysis method,<sup>[108]</sup> its depth penetration (typically  $\leq 10$  nm) is similar to the cross-sectional dimensions of individual CNCs. A recent method for estimating the detection limits for trace elements in a variety of elemental matrices provides a useful practical guide to estimating the level of impurity that can be detected.<sup>[109]</sup>

Low resolution XPS spectra of the carbon 1s and oxygen 1s peaks can be used to measure deviations from the carbon to oxygen atomic ratio of 1,2 for pure cellulose. More detailed analysis can be provided

by deconvolution of high resolution carbon 1s spectra at ~285 eV into the four component peaks due to different carbon bonding patterns as shown in [Figure 7](#): C1 for aliphatic carbons (C–C), C2 for C–O–C or C–OH in the glucose ring, C3 for O–C–O in the glucose ring and C4 due to esters (O–C = O) in the polymer chains. The presence of aliphatic sp<sup>3</sup> carbon (C–C/C–H) provides evidence for non-cellulose contaminants since cellulose contains only carbon bonded to oxygen, and an O–C–O to C–O intensity ratio approaching the theoretical value of 0,2 is indicative of pure cellulose.[\[47\]](#)[\[105\]](#) Similarly, the presence of carbon with three bonds to oxygen provides evidence for residual cell wall polysaccharides with carboxylic acid groups.[\[47\]](#)[\[105\]](#) Interestingly, in one case the polysaccharide contaminants could be removed by ethanol extraction.[\[105\]](#) In another example, high resolution spectra showed the presence of aliphatic carbons but the atomic ratio between cellulose carbon and oxygen was 1,2, as expected for pure cellulose, indicating adventitious contamination during storage or transport, rather than the presence of residual polysaccharides.[\[93\]](#) Beyond applications for detecting impurities and providing qualitative information on surface functional groups (e.g. carboxylates or sulfate half-esters, see [5.4](#)), XPS has frequently been used to analyse surface-modified CNCs by detecting nitrogen atoms or changes in the C/O ratio (see References [\[20\]](#), [\[47\]](#), [\[48\]](#), [\[92\]](#), [\[110\]](#)). XPS has also been used to detect other elements, such as silicon or silver.[\[106\]](#)[\[111\]](#)



#### Key

X energy (eV)

Y counts

SOURCE Labet and Thielemans 2011.[\[105\]](#)

**Figure 7 — XPS spectrum for sulfated cotton CNCs after deconvolution to separate peaks due to aliphatic carbon (C1, impurities), C-O-C (C2) and C-O-C (C3)**

## 6 CNC Morphology

### 6.1 Distributions of length and cross-section from microscopy

#### 6.1.1 General

The shape and size of individual CNCs can be assessed by imaging methods, such as scanning electron microscopy (SEM), transmission electron microscopy (TEM) and atomic force microscopy (AFM). These methods can be used to visualize individual particles and measure their size (length, width, height) and shape. Both electron microscopy (EM) and AFM require that the sample be deposited on a surface and yield the most reliable information for well-dispersed particles. Therefore, it is critical to provide details for sample preparation, including the dispersion procedure when starting

with dry samples. Agglomerated/aggregated particles are frequently detected by both EM and AFM; agglomeration/aggregation might result from the sample preparation method and does not necessarily reflect the distribution of agglomerates in the initial sample.[112][113][114] The following subclauses describe the basic method and sample preparation for EM and AFM, image analysis considerations and a summary of representative data obtained for CNCs.

### 6.1.2 Electron microscopy

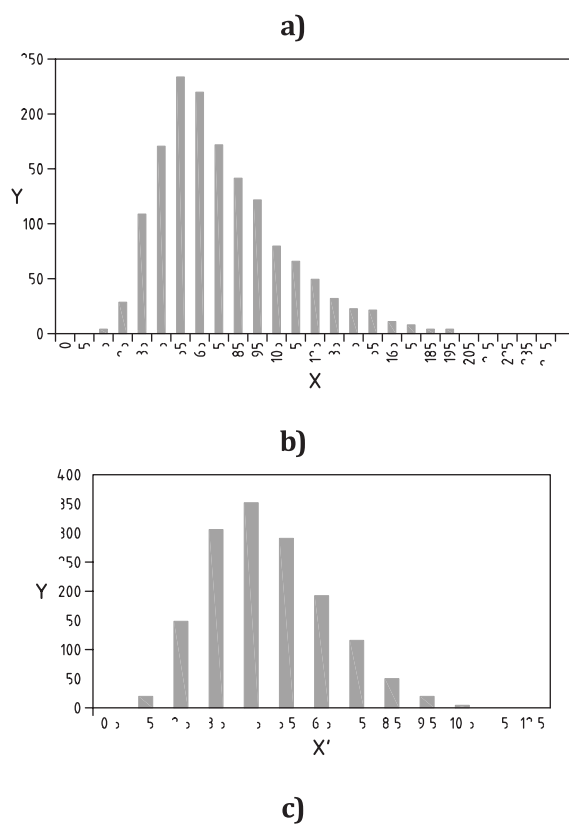
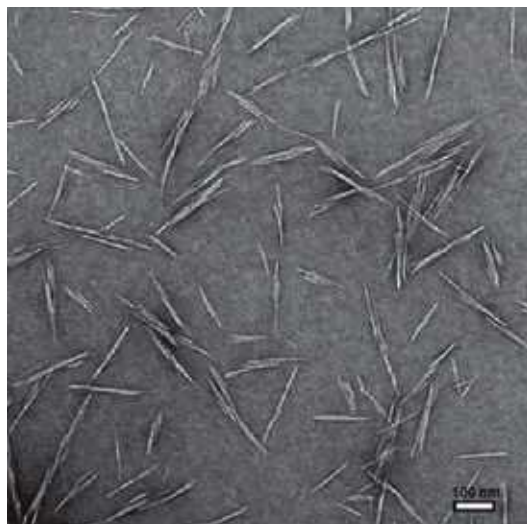
Electron microscopy (EM) uses a focused electron beam to visualize samples and measure their morphology and/or composition. Images are constructed based on collecting secondary or backscattered electrons from the surface of a thick sample for SEM, whereas in TEM the electrons that are transmitted through a thin sample are collected for image formation. This results in a 2D projection of 3D particles, which means that the length and width of particles can be determined, but not their height. Electron microscopes are typically operated under high vacuum for dry samples and heavy-atom-containing samples are needed for high contrast. SEM resolution is on the order of several nm and, therefore, its utility is limited for measuring the cross-sections of individual CNCs; however, it has been used in some cases for qualitative examinations of CNC morphology and for characterizing the large aggregates found in dry CNCs.[49][57][112][113][114] Modern field emission (FE) sources for SEM operated in scanning transmission mode provide some improvement in resolution, but TEM with its sub-nanometer scale resolution is the preferred method for obtaining both length and width distributions for CNCs.

Samples for TEM characterization are prepared from an aqueous suspension of CNCs diluted to ~0,01 % mass/volume (m/v). A small volume (5  $\mu$ L to 10  $\mu$ L) is deposited on an EM grid, incubated for several min and then blotted to remove excess liquid and washed several times with deionized water. Carbon-coated copper EM grids have been the most commonly used, although it might be advantageous to use a positively charged grid to facilitate immobilization of negatively charged CNCs. One study has reported that hydrophilic silicon oxide coated grids give better dispersed CNCs than either formvar or carbon-coated grids and that pH 3,5 is optimal for minimizing aggregation.[112] In most cases, negative staining with uranyl acetate has been used to improve contrast, although several TEM and cryo-TEM studies of unstained CNCs have also been reported.[22][79][112][115] One of these examples reported that with careful control of imaging conditions it was possible to obtain TEM images of sufficient quality to measure size distributions for unstained CNCs.[112] Sample staining is accomplished by either immersing the EM grid in an aqueous uranyl acetate solution (0,5 % to 2 % m/v) followed by washing with water, or by adding a small aliquot of the staining solution to the grid, waiting for 1 min to 2 min and then blotting the sample. Samples are dried in a clean, dust-free environment, taking care not to twist or rupture the coating. Samples for FE-SEM are prepared using similar grids and negative staining procedures.[38][113][116]

Most EM studies of CNCs have used a TEM equipped with a CCD camera with an operating voltage of  $\leq 200$  kV for high resolution imaging[3][5][6][7] or a FE-SEM operated between 10 kV to 30 kV. The microscope is calibrated using a standard of known size, such as polystyrene spheres, colloidal gold or calibration gratings. Certified calibration standards are preferred for this purpose. Methods for calibrating TEM image magnification using reference materials with periodic structures are available in ISO 29301.[117] The microscope should be carefully aligned in accordance with the manufacturer's recommendation to obtain accurate particle sizes and optimized for high resolution imaging. After installing the sample in the microscope chamber, several large field-of-view images of different sample areas are measured to verify that the sample quality is adequate. Samples with large numbers of individual particles and few agglomerates are ideal and might require some optimization of sample preparation conditions (e.g. type of grid, appropriate dilution of initial CNC suspension, incubation and wash procedures).

Multiple smaller field-of-view images (typically  $\leq 1 \mu\text{m} \times 1 \mu\text{m}$ ) are required for statistical analysis of particle dimensions. The combination of magnification and camera pixel size should be appropriate to ensure that individual CNCs are imaged with a sufficient number of pixels, while maximizing the number of particles per image. The image recording time should be long enough to give adequate signal to background while minimizing stage drift and sample damage. A sufficient number of images are recorded to interrogate a minimum of ~1 000 individual CNCs. A representative TEM image for CNCs is shown in [Figure 8](#) for a sample stained with uranyl acetate; individual and agglomerated CNCs are

evident in the image. Analysis of the data gives an average length of 76 nm and an average width of 5,0 nm with standard deviations of 32 nm and 1,7 nm, respectively.



**Key**

- X length (nm)
- Y counts
- X' width (nm)

SOURCE Cellulose Nanocrystal Reference Material Certificate (2014).[\[94\]](#)

**Figure 8 — Transmission electron microscopy image a) of CNCs derived from wood pulp and length b) and width c) histograms from analysis of ~1 500 particles**

### 6.1.3 Atomic force microscopy

Atomic force microscopy functions by scanning a sharp tip attached to a flexible cantilever across the sample surface. The movement required to maintain a constant deflection or oscillation amplitude of the cantilever, as it scans the surface is used to construct a 3D image. AFM provides both lateral dimensions and particle height. The lateral resolution of AFM is limited by the convolution of the tip geometry with the sample geometry, leading to a tip-broadening effect for measurement of features that are similar in size or smaller than the tip. Note, however, that particle heights are not subject to tip-convolution effects and can be measured accurately. The apparent width of individual CNCs measured by AFM is substantially larger than the actual width, particularly for smaller CNCs, such as those from wood pulps. For a pyramidal tip with a radius of curvature of 10 nm imaging a cylindrical feature with a diameter of 5 nm, the measured width will be ~15 nm. This approximation is based on [Formula \(2\)](#), where  $W$  is the measured width,  $r$  is the radius of the feature and  $R$  is the radius of curvature of the tip.[\[118\]](#)

$$W = 2 \left( r(r + 2R) \right)^{\frac{1}{2}} \quad (2)$$

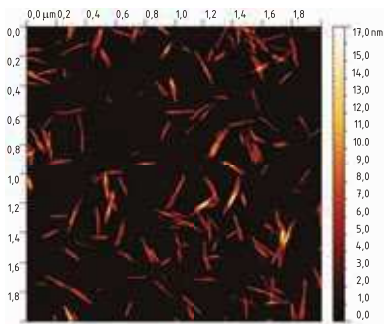
The tip broadening effect is small relative to the particle length for rod-shaped CNCs with lengths >100 nm (<10 %, depending on the length and height of the particles, the tip dimensions and the scan direction relative to the long axis of the CNC particle). Correcting for tip convolution effects requires that the tip size be measured, which has been accomplished in one case by co-depositing CNCs with 10 nm (mean diameter) gold nanoparticles as a reference.[\[119\]](#)

Sample preparation for AFM is similar to EM in that a dilute aqueous CNC suspension is deposited on a solid surface.[\[5\]\[9\]\[10\]\[11\]\[12\]\[13\]](#) Mica is the most widely used support due its low surface roughness over a large area and the availability of a clean surface that is generated by cleaving several surface layers immediately prior to use. The use of a positively charged surface, such as poly-lysine-coated mica, has advantages for the reproducible immobilization of the negatively charged CNCs.[\[21\]\[79\]\[94\]\[119\]\[120\]\[121\]](#) Uniform, positively charged surfaces can be prepared by dipping freshly cleaved mica in a dilute solution of poly-lysine for ~30 min, followed by washing with deionized water and drying. Dilute aqueous suspensions (dilution and amount vary with surface used) of CNCs are incubated with the surface for several min, washed by immersing in water to remove unattached material, and dried in a nitrogen stream or in a clean environment, such as a nitrogen-purged box. Alternate procedures of spin-casting or drop casting have been used for AFM sample preparation in a few cases.[\[79\]\[110\]](#) The sample deposition procedure requires optimization to minimize CNC agglomeration, as described above for EM. CNCs can also be imaged in an aqueous environment.[\[120\]](#) Although this might be advantageous for some applications, it does not provide particular advantages for routine assessment of the morphology of unmodified CNCs.

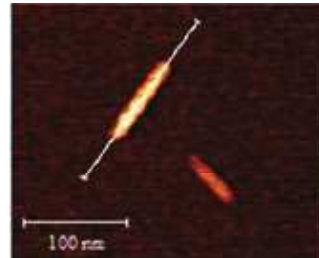
Imaging of CNC morphology requires an AFM that is compatible with measurements of particles with nanometer-scale dimensions. Intermittent contact mode operation (often referred to as tapping mode) is frequently used to minimize movement of the individual particles by the tip, although contact mode has also been employed for qualitative measurements. Probes with a radius of curvature of  $\leq 10$  nm are recommended in order to minimize tip-feature convolution. The applied force should be minimized and scan rate and gains optimized for imaging of small, loosely adsorbed particles. AFM has z-resolution on the order of 0,1 nm, thus providing accurate measurement of particle height, assuming that the force applied by the tip does not compress the sample. It is important to verify this by testing several applied forces. The AFM scanner calibration (x, y and z scales) should be verified by measuring a standard calibration grid; the z-step height should be comparable to the height of the particles to be measured. Detailed guidelines are provided in ISO 11952[\[122\]](#), ASTM E2530[\[123\]](#) and ASTM E2859[\[124\]](#).

Representative AFM images are shown in [Figure 9](#). Large scan areas (5  $\mu\text{m} \times 5 \mu\text{m}$  or 10  $\mu\text{m} \times 10 \mu\text{m}$ ) provide an assessment of the overall sample morphology and CNC distribution. Some microscopes are equipped with an optical microscope that can be used to assist with identification of suitable sample areas for AFM. Detailed size analysis for individual particles requires images that are 1  $\mu\text{m} \times 1 \mu\text{m}$  or smaller. Note that for an instrument with a typical 512 points/line scan a 1  $\mu\text{m} \times 1 \mu\text{m}$  image corresponds to ~2 nm/pixel. The number of images required will depend on the particle distribution and the number of individual particles required for analysis. Histograms for length [[Figure 9 d](#)] and height [[Figure 9 e](#)]

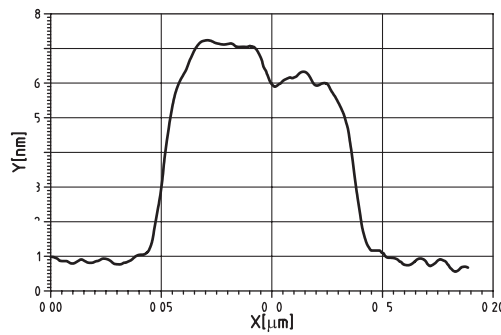
of 300 CNCs from three samples give mean values of  $5,0 \text{ nm} \pm 1,6 \text{ nm}$  and  $109 \text{ nm} \pm 46 \text{ nm}$ , respectively. Images often require flattening to remove artefacts prior to analysis.[125] Most AFM software includes an option to exclude nanoparticles while flattening the background.



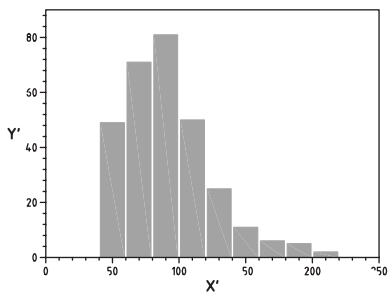
a)



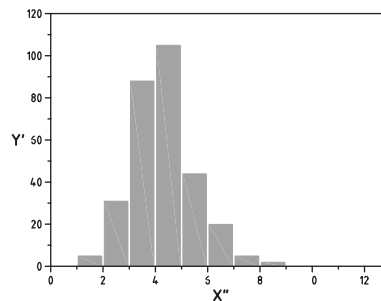
b)



c)



d)



e)

**Key**

- X length
- X' length (nm)
- X'' height (nm)
- Y height
- Y' counts

SOURCE Brinkmann et al. (2016).[126]

**Figure 9 — AFM images of CNCs a), b) derived from wood pulp, a cross section c) for one CNC and length d) and height e) histograms from analysis of 300 particles**



#### 6.1.4 Image analysis considerations

The measurement of a large number of individual particles is required to construct histograms of particle size. This is particularly important for CNCs which have a broader size distribution than some synthetic nanomaterials (e.g. gold nanoparticles). Information on methods for image and particle size analysis and sampling for microscopy is provided in ISO 9276[127] and ISO 13322-1[128]. It is important to ensure statistically representative sampling when employing microscopy methods that interrogate a very small fraction of the total sample. One recommendation is to split the original sample and measure at least three separate parts.[17][18] Additional guidelines for ensuring representative sampling are provided in ISO 14488[129]. An overview of the types of information that can be obtained from microscopy studies of nanomaterials and some of the general and technique-specific issues that should be considered are provided in a recent Technical Report; see ISO 14187[108].

The length of time required to analyse the dimensions of individual particles is frequently considerably longer than that required for data acquisition and is a significant limitation to acquiring size distributions based on large numbers of particles by microscopy. In some cases, it might be possible to use open source software, such as ImageJ or Gwyddion to automate the analysis procedure. This is typically accomplished by thresholding the image to identify particles for analysis and then excluding agglomerated particles. However, this approach is frequently unsatisfactory, since it requires that the image background be uniform and the sample free of contamination. The other main issue associated with image analysis is the frequent presence of agglomerated particles, which might be present in the initial suspension or might form when the sample is deposited on a surface. Although it is preferable to restrict analysis to individual (non-overlapping) CNCs, excluding large numbers of agglomerated particles increases the number of images required and increases the risk that the sampling is not representative. In practice, adjacent particles can only be analysed if the edges of individual particles are clearly defined. The choice of “analysable” particles unfortunately does introduce user bias into the analysis process. An additional factor to consider in analysing the height or width of CNCs is that the cross-section might vary along the length of the nanocrystal [see Figure 9 b) and Figure 9 c)]. A systematic approach (for example, reporting the maximum cross-section, based on either width or height) should be used in analysing individual particles.

One approach for reporting CNC size data is to plot histograms that illustrate the distribution of length and width and/or height; typically the mean (number average) and standard deviation (as a measure of the width of the distribution) are provided and the aspect ratio is calculated from the mean length and width (or height). Procedures for calculating mean sizes and standard deviations of size distributions for histogram data are summarized in ASTM E2578-07[130]. Considering the above image analysis recommendations, it is important to provide information on the number of particles that are analysed and also on the procedure for dealing with agglomerated CNCs. Representative histograms for TEM ( $n = 1\,500$ ) and AFM ( $n = 300$ ) data are shown in Figures 8 and 9 for a wood pulp CNC sample. For most cases where a relatively large number of particles have been measured, the histograms can be adequately fitted by a log normal distribution.

#### 6.1.5 Microscopy size distributions for CNCs

TEM and AFM have been used extensively to measure lengths and widths/heights for CNCs from a variety of cellulose sources. In many cases, data are based on analysis of a limited number of images/particles and an average or range of dimensions is provided; rarely are full details on the number of particles analysed and the analysis procedures provided. Summaries of this (qualitative) data and references to the primary literature can be found in several recent reviews.[2][8] This subclause focuses on a subset of more detailed microscopy studies where larger numbers of particles are analysed and histograms of size distributions (number-based) are provided along with mean values and standard deviations. A selection of representative data are summarized in Table 3.

There are a number of trends in the data in Table 3, and previous reviews. [2][8] First, CNCs show distinct nanorod morphologies, with dimensions that vary substantially depending on the cellulose source and the extraction process. Wood pulp CNCs have been the most extensively studied and have average cross-sections between 4 nm and 9 nm and average lengths of 100 nm to 200 nm. Other plants, such as sisal and ramie have similar dimensions, but cotton CNCs typically have significantly larger cross-sections. Bacterial and tunicate CNCs are substantially larger with average cross-sections  $\leq 50$  nm and

10 nm to 20 nm and average lengths  $\leq 1 \mu\text{m}$  and  $1 \mu\text{m}$  to  $3 \mu\text{m}$ , respectively. Several studies[21][22][23][24][26] have examined the effects of the production process on the CNC size. An AFM study measured CNC lengths and heights for  $\sim 300$  individual nanocrystals for softwood pulps[21] as a function of hydrolysis time and acid /pulp ratios. The average CNC length varied from 105 nm to 141 nm and the height varied from 4,5 nm to 5,0 nm, with reduced length and cross-section for longer hydrolysis times and higher acid/pulp ratios. A similar study of cotton CNCs also demonstrated a reduction in length for higher temperature hydrolysis.[22] This study concluded that the length and width were correlated, with longer particles being wider. Although this does not appear to have been examined in other studies, it might have implications for modelling dimensional data obtained by light scattering (see 6.2). The drying method had little effect on the dimensions of wood CNCs,[23] although it did affect the ability to obtain well-dispersed samples.[24] Finally, the dimensions of wood pulp CNCs with carboxylated surfaces are within the range obtained for those with sulfate half-esters at their surfaces.[16][50]

A second trend is that the size distributions are broad, as observed by qualitative inspection of individual images and quantified by the standard deviation of the distribution. As illustrated in Table 3, standard deviations of 30 nm to 70 nm and  $>1,5 \text{ nm}$  are common for length and width, respectively, of plant-based CNCs. This is consistent with ensemble measurements using dynamic light scattering for which polydisperse size distributions are obtained (6.2). The broad distributions mean that it is challenging to differentiate between populations of CNCs with similar size distributions. Note that the size distribution is somewhat broader for length as compared to width/height (the standard deviation is typically  $\geq 40 \%$  of the mean length, but a smaller fraction of the mean cross-section, Table 3).

A third observation is that agglomeration of particles is a significant problem; it can be minimized (but never eliminated) by sample dilution and/or sonication and by choice of charged surfaces or grids for CNC immobilization. It is difficult to distinguish agglomerates that form during sample deposition from those that are pre-existing in the sample; however, careful comparison of particle counting and ensemble measurements, such as light scattering might provide some insight. Although it is preferable to analyse only individual CNCs, this leads to exclusion of large (and variable) numbers of touching particles. This has a practical limitation in that many more images are necessary to achieve the required particle count. It might be a more serious issue if agglomeration depends on particle size, for example, if large particles have a greater tendency to agglomerate, the size distribution based on individual CNCs will be skewed towards smaller particles. This factor has, to the best of our knowledge, not yet been addressed.

The fourth observation is that CNC particles are irregularly shaped. This is obvious from TEM images in which the ends of the particles are smaller than the middle, a tapered, spindle-like structure that is responsible for the use of the term cellulose “whiskers”. Irregularly shaped particles are also evident in high resolution AFM images, which demonstrate that the height varies by up to several nm along the long axis of the particle (Figure 9, see References [22], [73], [113], [131], [132]). This might be due to incomplete hydrolysis of the amorphous regions between crystals or removal of parts of individual crystalline regions during the hydrolysis process. It appears that CNCs extracted by acid hydrolysis are usually composed of several elementary crystallites,[2][22] This is consistent with XRD measurements which estimate an average particle length of  $\sim 20 \text{ nm}$ , which is  $>5$  times shorter than the average lengths measured by microscopy for wood pulp derived CNCs.[2] Note that the estimated cross-sections of 3 nm to 5 nm from XRD are similar to those obtained by microscopy.

Table 3 — Sizes (nm) for CNCs from various cellulose sources and extraction methods

Cellulose source	Production method <sup>a</sup>	Method, conditions <sup>b</sup>	Average length (standard deviation)	Average cross-section <sup>c</sup> (standard deviation)	N <sup>d</sup>	Reference
Wood pulp (black spruce)	45 °C, 64 % H <sub>2</sub> SO <sub>4</sub> , 25 min, A/P = 8,75	AFM, PLL-mica, contact	141 (60)	5,0	~320	[21]
Wood pulp (black spruce)	45 °C, 64 % H <sub>2</sub> SO <sub>4</sub> , 45 min, A/P = 8,75	AFM, PLL-mica, contact	120 (45)	4,9	~325	[21]
Wood pulp (black spruce)	45 °C, 64 % H <sub>2</sub> SO <sub>4</sub> , 25 min, A/P = 17,5	AFM, PLL-mica, contact	105 (36)	4,5	~270	[21]
Wood pulp	(US FPL)	AFM, PLL-mica, TM		6,4 (h) 7,8 (w) <sup>e</sup>	100	[119]
Softwood kraft pulp	45 °C, 64 % H <sub>2</sub> SO <sub>4</sub> , 25 min, 2 % consistency; never-dried	AFM, titania-coated silicon, TM	63 (53)	4,4	>10 <sup>4</sup> f	[23]
Softwood kraft pulp	45 °C, 64 % H <sub>2</sub> SO <sub>4</sub> , 25 min, 2 % consistency; dry at 110 °C	AFM, titania-coated silicon, TM	53 (31)	4,3	>10 <sup>4</sup> f	[23]
Bleached softwood kraft pulp	FPIinnovations	FE-SEM, + grid, UA	116 (48)	Approximately 9 nm (limited resolution)	1 230	[116]
Softwood kraft pulp	H <sub>2</sub> SO <sub>4</sub> , FPIinnovations	AFM, PLL-mica, TM	109 (46)	5,0 (1,6)	300	[94]
Softwood kraft pulp	H <sub>2</sub> SO <sub>4</sub> , FPIinnovations	TEM, C-C grid, UA	76 (32)	5,0 (1,7)	1 500	[94]
Wood pulp	H <sub>2</sub> SO <sub>4</sub> , 45 °C, 60 min	TEM, C-C grid	211 (70)	8,8 (5,5)	200	[24]
		TEM, silicon oxide coated grid	149 (73)	5,2 (1,6)	200	[24]
		TEM, C-C grid, UA	248 (72)	9,1 (3.2)	200	[24]
Kraft eucalyptus pulp	56 °C, 58 % H <sub>2</sub> SO <sub>4</sub> , 40 min,	TEM, C-C grid, UA	174 (125)	10,7 (8,5)	510, 623 (l, w)	[26]
Wood pulp	64 % H <sub>2</sub> SO <sub>4</sub> (US FPL)	AFM, PLL-mica, TM	130 (67)	5,9 (1,8)	~400	[79]
Bacterial	60 °C, 3 7 % H <sub>2</sub> SO <sub>4</sub> , 48 hr	AFM, PLL-mica, TM	1 103 (698)	14,0 (7,4)	~430	[79]

<sup>a</sup> A/P is acid to pulp ratio.

<sup>b</sup> PLL-mica is poly-lysine coated mica; TM = tapping mode AFM; UA = uranyl acetate staining; C-C grid, carbon-coated copper grid.

<sup>c</sup> Height for AFM and width for EM, unless otherwise noted. Standard deviations are listed only when available in the literature reference.

<sup>d</sup> N values estimated from histograms in literature references are indicated with “~”.

<sup>e</sup> After deconvolution using gold nanospheres to measure tip size.

<sup>f</sup> Automated analysis.

<sup>g</sup> Height of 7,3 nm measured by AFM.

Table 3 (continued)

Cellulose source	Production method <sup>a</sup>	Method, conditions <sup>b</sup>	Average length (standard deviation)	Average cross-section <sup>c</sup> (standard deviation)	N <sup>d</sup>	Reference
Tunicate	48 % H <sub>2</sub> SO <sub>4</sub> ,	AFM, PLL-mica, TM	1 187 (1 066)	9,4 (5,0)	>500	[79]
Cotton linters	45 °C, 65 % H <sub>2</sub> SO <sub>4</sub> , 30 min	TEM, C-C grid, UA	141 (39)	27 (52) <sup>g</sup> 14 (57) cryo-TEM	>800	[22]
Cotton linters	72 °C, 65 % H <sub>2</sub> SO <sub>4</sub> , 30 min	TEM, C-C grid, UA	105 (47)	21 (52)	>800	[22]
Microcrystalline cellulose (wood pulp)	72 °C, 65 % H <sub>2</sub> SO <sub>4</sub> , 30 min	TEM, C-C grid, UA	105 (35)	12 (42)	>800	[22]
Microcrystalline cellulose (cotton)	44 °C, 62 % H <sub>2</sub> SO <sub>4</sub> , 30 min	AFM, mica, TM	246 (128)	5,9 (2,3)	—	[73]
Cotton fibres	55 °C, 65 % H <sub>2</sub> SO <sub>4</sub> , 30 min	TEM, C-C grid, UA	140 (15)	14,3 (2,0)	—	[91]
Ramie fibres	55 °C, 65 % H <sub>2</sub> SO <sub>4</sub> , 30 min	TEM, C-C grid, UA	185 (25)	6,5 (0,7)	—	[91]
Sisal fibres	55 °C, 65 % H <sub>2</sub> SO <sub>4</sub> , 30 min	TEM, C-C grid, UA	115 (21)	5,0 (1,5)	—	[91]
Sisal fibres	50 °C, 65 % H <sub>2</sub> SO <sub>4</sub> , 40 min	TEM, C-C grid, UA	215 (67)	5,0 (1,5)	425, 2 015 (l, w)	[133]
Wood pulp	Ammonium persulfate	AFM, TM	124 (41)	6,0 (1,7)	200, 253 (l, w)	[16]
Wood pulp	Ammonium persulfate	AFM, PLL-mica, TM	109 (46)	6,9 (3)	100	[50]

<sup>a</sup> A/P is acid to pulp ratio.

<sup>b</sup> PLL-mica is poly-lysine coated mica; TM = tapping mode AFM; UA = uranyl acetate staining; C-C grid, carbon-coated copper grid.

<sup>c</sup> Height for AFM and width for EM, unless otherwise noted. Standard deviations are listed only when available in the literature reference.

<sup>d</sup> N values estimated from histograms in literature references are indicated with “~”.

<sup>e</sup> After deconvolution using gold nanospheres to measure tip size.

<sup>f</sup> Automated analysis.

<sup>g</sup> Height of 7,3 nm measured by AFM.

The width of CNCs is not always equal to the height, as is evident for the long, high aspect ratio tunicate CNCs which have a ribbon structure with a helical twist.[22] A detailed AFM, TEM and cryo-TEM study reported that CNCs derived from cotton and wood pulp also differed in length and width, leading to the conclusion that most CNCs were composed of laterally associated individual crystallites.[22] The authors hypothesized that previous studies showing smaller widths were most likely measuring individual crystallites, rather than laterally bound crystallites. Based on the predicted crystal structures for wood pulps, one expects a square cross-section with width equals height in the 3 nm to 5 nm range, consistent with most EM and AFM data. In one case, it has been suggested that the width is 1,4 nm larger than the mean height, suggesting unequal short axis lengths.[119] However, the width was determined from deconvolution of AFM data, which might introduce additional errors in the measurement.

The largest amount of data in [Table 3](#) is for wood pulp-derived CNCs and, for the most part, the data from different laboratories are in reasonable agreement. With a few exceptions, the cross-section is approximately 5 nm and the lengths vary from 80 nm to 140 nm. CNCs from other plant sources, such as sisal and ramie have a similar size. The agreement for CNCs prepared and measured in different laboratories with different methods and sample preparation procedures indicates that applying standard data acquisition and analysis protocols to the same sample should generate results consistent with development of technical specifications.

There are relatively few examples, where the same sample has been assessed by both AFM and EM. One study used AFM, field emission SEM, and TEM to characterize CNCs isolated from microcrystalline cellulose, showing qualitative agreement between the three methods, although a quantitative analysis was not provided.<sup>[113]</sup> In another example, EM and AFM both gave average cross-sections of 5 nm, but the average length varied by 30 nm.<sup>[94]</sup> This might reflect differences in sample preparation between the two methods or between different laboratories. AFM and TEM can provide complementary information since TEM provides particle width while AFM provides particle height. Because of the tip-broadening effects, it might be advisable to obtain only height measurements from AFM and rely on EM for measurements of CNC width and length. Nevertheless, the sample staining used to enhance contrast in most EM measurements of CNCs has been suggested to increase particle agglomeration.<sup>[22][112]</sup> Finally, the choice of microscopy techniques will frequently be determined by cost and availability. AFM can be readily combined with either force spectroscopy to obtain mechanical properties or with optical (fluorescence, Raman) microscopy for correlated measurement of the same sample area on a single integrated microscope platform. Such approaches should be particularly valuable for characterization of chemically modified CNCs and composite materials containing CNCs, although these materials are outside the scope of this Technical Report.

## 6.2 Size measurement by dynamic light scattering (DLS)

Dynamic light scattering measures the time-dependent fluctuations in intensity of light scattered from particles suspended in liquid and undergoing Brownian motion. These intensity fluctuations are directly related to the rate of diffusion of the particle through the solvent and can be used to determine the translational diffusion coefficient, which is proportional to particle size, as well as the hydrodynamic diameter of the particle. For a non-spherical particle, one obtains the equivalent hydrodynamic diameter which is the diameter of a rigid sphere that diffuses at the same rate as the analyte particle. DLS is an ensemble method (compared to the particle counting approach used in microscopy, [6.1](#)) and calculates sizes based on simultaneous analysis of a large number of particles. It is a simpler, less expensive and more widely accessible method than either EM or AFM and can therefore be readily implemented for quality control and routine measurements. However, the intensity-weighted equivalent hydrodynamic diameter,  $d_h$ , of solvated particles estimated from DLS will almost always differ from the diameter measured by microscopic methods. For spherical particles, the differences are primarily due to the electrical double layer, whereas the situation will be more complex for other particle shapes, such as nanorods.

Measurement of nanoparticle size distributions by DLS is well-established and the general methods and data analysis are described in several standards and protocols. <sup>[134][135][136]</sup> For CNCs, samples diluted to a mass fraction of 0,05 % in 5 mmol/L to 10 mmol/L NaCl are typical. The use of a lower NaCl concentration might prevent gelation or agglomeration phenomena. It is important to avoid contamination (e.g. dust particles) of the sample, cuvettes or NaCl solution due to the much larger scattering intensity from larger particles; the suspension should be filtered to remove such particles. The scattering intensity is proportional to  $r^6$  (where  $r$  is the radius of the scattering particle) which means that the scattered intensity from a 100 nm particle will be one million times larger than that from a 10 nm particle. Typically, a minimum of three measurements (which are each averages of several readings, the exact number typically being automatically selected by the instrument data acquisition software) per sample should be obtained and an equivalent blank sample (without CNCs) should be measured to check for background scattering.

The raw data (light scattering intensity fluctuations) are plotted as a correlation function from which the translational diffusion coefficient,  $D_t$ , is obtained. ISO 22412<sup>[134]</sup> recommends use of the Cumulants analysis method which fits the data to a polynomial expansion to obtain  $D_t$ . The Stokes Einstein

Formula (3), where  $k$  is the Boltzmann constant,  $T$  is the temperature in K and  $\eta$  is the viscosity of the medium, is then used to calculate the mean hydrodynamic diameter,  $d_h$ :

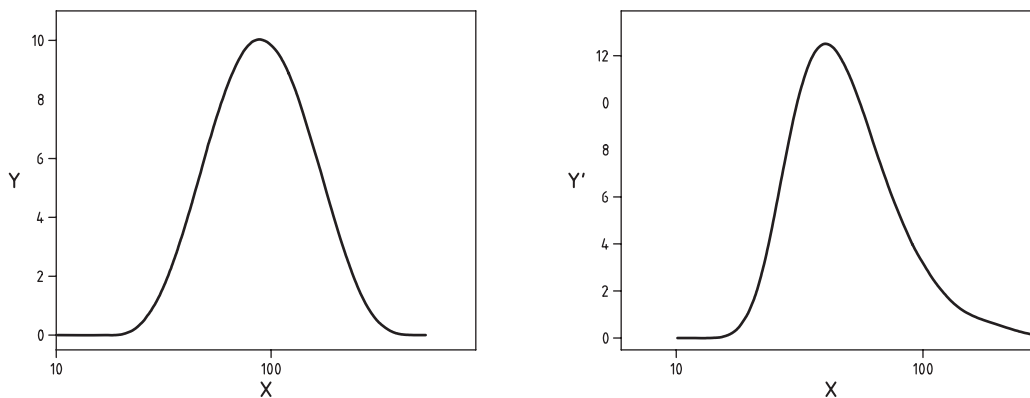
$$d_h = kT / 3\pi\eta D_t \tag{3}$$

This calculation requires accurate values for the temperature (usually provided by the instrument software) and the viscosity and refractive index of the liquid (e.g. 5 mmol/L NaCl solution) in which the particles are suspended for calculation of the diffusion coefficient. The fit of the correlation function also provides the polydispersity index, PI, which is a dimensionless measure of the broadness of the size distribution.[134] For a single Gaussian distribution, PI, is defined by Formula (4) where  $\sigma$  is the standard deviation and  $d_h$  is the mean size (expressed as equivalent hydrodynamic diameter):

$$PI = \sigma^2 / d_h^2 \tag{4}$$

Note that data fits using the Cumulants approach give only the intensity-weighted mean and PI, not the actual size distribution.

DLS provides intensity-weighted distributions that differ from the number-weighted distributions obtained from particle counting methods. The fact that CNCs are considerably polydisperse in at least one dimension (length) further complicates their measurement by this method. Since the scattering intensity is proportional to  $r^6$ , the contribution of light scattered from small particles might be a very small fraction of the total intensity and larger particles might further screen the light scattered from the smaller ones. Smaller particles are thus difficult to quantify accurately, affecting the accuracy of the particle size distribution measured by DLS. It is possible to convert the intensity distribution to a volume distribution using Mie scattering theory and the refractive index of the particle. The volume distribution has the advantage of more clearly showing signals due to small particles that have low scattering intensity and is shifted to lower apparent diameter, as shown by the intensity and volume plots in Figure 10. The practical difficulties associated with this conversion are discussed in a recent ASTM standard which does not recommend further conversion to a number distribution.[135]



**Key**

- X      equivalent hydrodynamic diameter (nm)
- Y      intensity (%)
- Y'     volume (%)

SOURCE Cellulose Nanocrystal Reference Material Certificate (2014).[94]

**Figure 10 — Dynamic light scattering data for CNCs in 5 mmol/L NaCl showing intensity (left) and volume (right) plots**

The standard Cumulants method for extracting size information from DLS works well for monodisperse samples (PI < 0,1). Although several algorithms have been used to fit correlation curves to extract multiple components for polydisperse samples (summarized in Reference [135]), there is so far no generally accepted method for analysing such samples. Methods and limitations for extraction of bimodal

or multimodal distributions of particle sizes have been reported for spherical latex particles<sup>[137][138]</sup> and it is likely that dealing with highly polydisperse samples will be even more problematic for non-spherical particles, such as CNC nanorods.

Representative DLS data for wood pulp CNCs are provided in [Figure 10](#), with  $d_h = 78,5$  nm and a PI of 0,21. The measured equivalent hydrodynamic diameter represents the size of a sphere that would diffuse at the same rate as the CNCs, but additional information is required to convert this number to the actual CNC dimensions. For non-spherical particles, such as the high aspect ratio CNCs, the scattered light will have an angular dependence due to rotational motion, requiring measurement of the rotational diffusion coefficient. Despite this limitation, DLS has been used as a qualitative method to measure  $d_h$  to track size changes for CNCs prepared by different methods and with differing surface functionality/counterions.<sup>[29][40][48][54][132][139][140]</sup> A similar approach has also been used to validate procedures for redispersion of dry CNCs<sup>[28]</sup> and to evaluate the effect of storage conditions on the physico-chemical stability of dry and suspended CNCs.<sup>[96]</sup> In cases where DLS results have been compared to microscopy size measurements, similar trends are observed for changes in  $d_h$  and length.<sup>[139][140]</sup>

Several approaches have been explored to deal with the problem of obtaining informative particle size distributions from light scattering data for rod-shaped CNCs, particularly the particle length and axial ratio. A combination of polarized and depolarized dynamic light scattering has been used to obtain rotational and translational diffusion coefficients for cotton CNCs.<sup>[141]</sup> The Broersma formulae which relate the translational and rotational diffusion coefficients to the rod length and the ratio of the rod length to its cross-section were used to calculate the average CNC dimensions (length, diameter). This gave estimates that were in reasonable agreement with the average CNC sizes measured by TEM, although sample polydispersity was a complicating factor in some cases. Multi-angle light scattering has also been employed to obtain length distributions.<sup>[142][143]</sup> In this method, the angular dependence of the scattered light intensity is used in combination with the theoretical form factor for a rod to obtain the CNC length *distribution* (or average dimensions and polydispersity index). A more detailed approach that accounts for the effect of aspect ratio, shape and polydispersity has also been published recently.<sup>[144]</sup> Another recent report has taken the potentially simpler approach of using the translational diffusion coefficient from DLS measurements and an average CNC cross-section measured by microscopy to obtain the mean particle length, assuming a cylindrical rod,<sup>[145]</sup> as also mentioned briefly in an earlier study.<sup>[146]</sup> This method might be sufficient to obtain qualitative data on particle length, since the translational diffusion coefficient depends more strongly on particle length than cross-section and the CNC cross-section is less variable than the length. Note that all these approaches require assumptions about the CNC shape. Based on microscopy data, the CNC length and cross-section vary substantially along the long and short axes, respectively, and might also differ from the ideal square or rectangular cross-section predicted from crystallography data.

Finally, a recent study has compared CNC size estimates from electron microscopy to those obtained by light scattering and nanoparticle tracking.<sup>[116]</sup> CNC aspect ratios were estimated from translational diffusion coefficients obtained by DLS, assuming both ellipsoidal and cylindrical shapes, and were in good agreement with EM data. The DLS and EM data were also compared to data from nanoparticle tracking analysis. This non-imaging particle counting method tracks light scattered from individual particles moving under Brownian motion to follow their dynamics and provides a number-based size distribution. The volume-weighted CNC radius estimated from DLS was 22 nm, as compared to a number-weighted radius of 37 nm from particle tracking; the apparent size discrepancy was suggested to be caused by sample polydispersity and inherent differences between the two methods. Although this appears to be the only example in which particle tracking was applied to CNCs, this method has the potential advantage of providing number-based distributions that can be compared with microscopy data and that might better resolve the broad length distribution.

## 7 CNC Surface characteristics

### 7.1 Specific surface area

The specific surface area of dispersed particles, either dry or in suspension, is an important parameter for characterization of any nanomaterial. For CNCs, the surface area provides information on the

dispersibility of the material and the available surface area for modification to incorporate functionality (e.g. for catalysis applications or incorporation in composite materials).

The specific surface area of solids is typically determined by measuring the amount of physically adsorbed gas according to the Brunauer-Emmett-Teller (BET) method for interpreting gas adsorption isotherms. ISO 9277[147] provides details on the determination of overall specific external and internal surface areas of dispersed or porous solids; dry samples are degassed at elevated temperature (>100 °C) before measuring adsorption of gas, usually nitrogen. Although, the BET method has been applied to some nanomaterials, complications related to particle agglomeration and/or aggregation have also been noted.[148][149] CNCs typically form relatively large tightly-packed agglomerates and aggregates (dimensions of  $\mu\text{m}$  or larger) when dried[112][113][114] and the extensive degassing at elevated temperatures that precedes gas adsorption when using the BET method might cause further aggregation or degradation of the cellulose. Therefore, surface areas measured for dry agglomerated or aggregated CNCs are much lower  $\sim 1 \text{ m}^2/\text{g}$ [34][94] than values estimated by calculating the surface area based on average CNC dimensions (e.g.  $419 \text{ m}^2/\text{g}$  for CNCs with dimensions of  $6 \text{ nm} \times 6 \text{ nm} \times 180 \text{ nm}$ , see Reference [150]). This indicates that measuring a specific surface area for dry, dispersed CNCs using the BET method will require the development of a drying method that prevents aggregation of individual particles.

Measurement of the surface area for CNC suspensions, rather than dry material, might frequently be more relevant since it provides the accessible surface for reaction in solution or for formulation in composite materials. A solution method based on adsorption of Congo red dye that has been employed to measure specific surface areas of bacterial and microfibrillated cellulose[151] was recently used for CNCs. Wood pulp and bacterial CNCs prepared by sulfuric acid hydrolysis gave values of  $249 \text{ m}^2/\text{g}$  and  $272 \text{ m}^2/\text{g}$ , within the expected range for typical CNCs.[152] Two NMR methods that have been used for cellulosic materials or nanoparticles might also be useful approaches. The first employs CP-MAS  $^{13}\text{C}$  solid state NMR to measure the ratio of inaccessible and accessible signals for the disordered C4 carbons for hydrated cellulosic materials [Figure 6 b)]. This ratio can be used to calculate the surface area, assuming a rectangular particle shape and using the known density of cellulose.[153] For a never-dried dissolving pulp, this NMR method provided a specific surface area that was twofold larger than the value determined by the BET method for a sample dried by a solvent exchange method, in which the water was replaced by a series of successively less polar solvents before final drying under argon.[153] A similar CP-MAS NMR approach has been used to examine the role of the drying method in controlling the lateral aggregation of cellulose fibrils and hence the surface area available for functionalization.[154] Adapting this method to evaluate the specific surface area of never-dried or redispersed CNCs gave values[126] that were in reasonable agreement with calculated surface areas using average CNC dimensions from microscopy and the range of internal specific areas measured by the BET method for CNC aerogels ( $216 \text{ m}^2/\text{g}$  to  $605 \text{ m}^2/\text{g}$ ).[150]

A second NMR approach that has been applied to suspensions of nanomaterials[155] takes advantage of the much shorter relaxation time for liquids on a particle surface compared to the bulk liquid. The measured solvent relaxation time is a weighted average of the surface and bulk relaxation times, weighted by the relative amounts of surface and bulk liquid. Although NMR relaxation times have been used to examine interactions of cellulose with a variety of plant wall components and to provide information on cell wall pore volume to surface area,[65] the method has not yet been applied to CNC surface area measurements. NMR relaxation times can be measured on a routine solution NMR or bench-top instrument, making this a potentially easy to use and accessible method. To date, neither NMR approach has been sufficiently widely used to assess whether it will be a generally useful method for measuring the specific surface area of CNCs or other cellulosic nanomaterials.

## 7.2 Surface charge

The CNC surface charge is frequently estimated from zeta potential measurements. Zeta potential is defined as the difference between the electrical potential of the bulk liquid and that of the stationary layer of fluid attached to the dispersed particles (i.e. the slipping plane which is the region of the liquid-solid interface where the liquid starts to slide relative to the surface under the influence of shear stress).[156] It is a model/method dependent value that is derived from electrophoretic mobility and is a metric for the surface potential or the degree of electrostatic forces acting between two charged particles or a charged particle and a surface. The electrophoretic mobility,  $U_E$ , [156] is measured by applying a potential



across two electrodes in a sample cell and measuring the movement of charged particles towards the oppositely charged electrode (cathode or anode) as a function of the applied electric field. Although particle mobility was initially measured by monitoring the movement of individual particles by video microscopy, it is now more common to use electrophoretic light scattering. This is an ensemble method, similar to dynamic light scattering, in which  $U_E$  is measured from the Doppler shifts in the frequency of scattered light from the particle moving in the applied field. The theoretical background and methods for obtaining the electrophoretic mobility are described in ISO 13099-1[156] and ISO 13099-2[157] and references within them. Practical guides for measuring  $U_E$  and zeta potential for biological materials and nanoparticles are also available.[158][159]

A key consideration for zeta potential measurements is that the calculated value is a function of both the particle and its surrounding solution. Methods for measuring  $U_E$  assume unrestricted mobility of the particles and the values obtained depend on the pH, temperature, particle concentration, ionic strength of the dispersing solution and the presence of polyvalent ions. Therefore, a zeta potential measurement has little value unless all relevant parameters are reported. Electrophoretic mobility can be used to determine zeta potential using [Formula \(5\)](#), where  $\epsilon$  and  $\eta$  are the dielectric constant and viscosity of the medium. The term  $f(\kappa\alpha)$ , known as Henry's function, is related to the ratio of the particle radius to the electrical double layer thickness and varies between 1,0 and 1,5. For large particles in aqueous suspension a value of 1,5 is typically assumed (Smoluchowski approximation) whereas for small particles in organic liquid a value of 1 is used (Huckel approximation).[158]

$$U_E = (\epsilon \times \text{zeta potential} \times f(\kappa\alpha)) / 6\pi\eta \quad (5)$$

Measurement of zeta potential from  $U_E$  for CNCs has been frequently used to assess the colloidal stability and to measure the electrical charge on the nanocrystals, both of which are related to the presence of charged functional groups. Note that the number of titratable surface groups measured by conductometric titration (see [5.4](#)) can be converted to an equivalent charge density if the surface area is known. Zeta potential measurements have typically used dilute CNC suspensions (0,05 % to 1,0 %) in deionized water, in some cases with added NaCl. The sample preparation is similar to that for DLS (see [6.2](#)) and it is particularly important to filter samples and ensure that additional ions or contaminants are not introduced during sample dilution or measurement. Several studies have reported values of zeta potential between -40 mV and -60 mV for sulfated CNCs produced by sulfuric acid hydrolysis of wood pulp, rice straw and filter paper.[20][49][90][132][139][160] These experiments include data for both protonated and sodium form CNCs at approximately neutral pH and in the absence of added salt. The data are consistent with a stable suspension of charged particles. As a general guideline, suspensions with negatively charged particles that have zeta potentials of -30 mV to -40 mV are considered moderately stable while values of -60 mV to -80 mV indicate very good stability.[158] In one recent study, the effects of NaCl on sulfated softwood pulps were assessed; zeta potentials decreased from -62,8 mV in deionized water to approximately -20 mV in the presence of 10 mmol/L NaCl, clearly showing the significant effect of added sodium ions.[132] In another example, the zeta potentials for cotton-derived CNCs varied with their sulfur content, with more negative values measured for CNCs with higher sulfur content.[161] Lower values (-2 mV to -30 mV) were obtained for cotton CNCs[161][162] than for the other plant-derived CNCs mentioned above, although it is problematic to compare results of different studies since there are frequently differences in conditions and possibly also in the approximations used to calculate zeta potential.

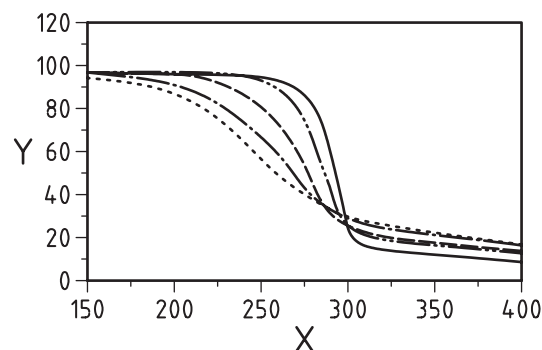
## 8 Miscellaneous

### 8.1 Thermal properties

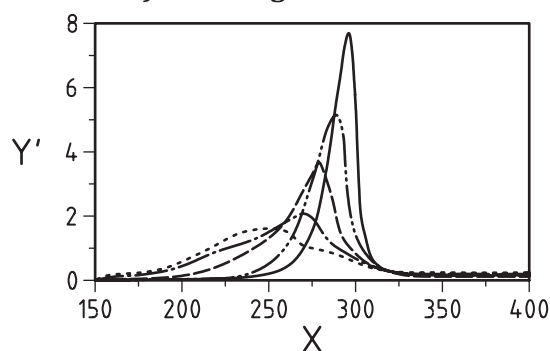
The thermal stability of CNCs is an important factor for some applications, for example, in the production of CNC nanocomposites which frequently require a thermal processing step. Thermal stability is typically measured by thermogravimetric analysis (TGA), a method that measures the mass of a sample while heating at a controlled rate in either an inert or oxidizing atmosphere. This method can be used in dynamic mode where the mass change is measured as a function of temperature under controlled heating conditions or in isothermal mode where the mass change at a specific temperature is measured as a function of time. There are published ISO and ASTM standards[163][164][165][166] that

outline general methods and calibration procedures for TGA of a variety of materials, with those for polymers and carbon nanotubes<sup>[165][166]</sup> being the most relevant to CNCs. Certified reference materials should be used for calibration of both the mass scale and temperature. Typical TGA experiments for CNCs use 5 mg to 20 mg of dry sample, with a flow of either nitrogen or air and a heating rate of 2 °C to 10 °C from room temperature to  $\geq 500$  °C.

Most TGA measurements of CNCs have used dynamic mode with the data plotted, as either a thermogram or a differential thermogram and frequently the data are compared to those for the cellulose biomass source.<sup>[24][52][90][95][161][167][168][169]</sup> Results are reported in several ways, including the temperature for the onset of mass loss, the temperature for maximum change in mass and the % char remaining at a specified temperature. The shape of the TG curves and the onset of mass loss will vary depending on the type of cellulose particle, the surface functional groups, the heating rate and atmosphere (air vs nitrogen). A study of bacterial cellulose prepared by sulfuric acid hydrolysis under various conditions provides a useful overview of the typical trends observed in the literature ([Figure 11](#)).<sup>[95]</sup> The unhydrolyzed bacterial cellulose showed a modest mass decrease at low temperatures due to loss of water, followed by a major change between 250 °C and 325 °C, which was attributed to cellulose degradation processes, such as dehydration, depolymerization and decomposition of sugars, followed by formation of a char residue. Further decomposition of the residue occurs above  $\sim 425$  °C and was assigned to oxidation and formation of low weight gaseous products. The mass loss occurred at lower temperatures and over a broader temperature range as the CNC sulfate half ester content increased. These results have been attributed to a combination of two processes: the degradation of the sulfated regions of the CNCs occurs at lower temperature, possibly with catalysis of the dehydration reactions by the acidic sulfate half ester groups, and is followed by the decomposition of the unsulfated interior of the crystal at higher temperatures.



a) Thermogravimetric



b) Derivative thermogravimetric

**Key**

- X      temperature (°C)  
 Y      weight (%)  
 Y'     derivative (%·min<sup>-1</sup>)

SOURCE Maren and Winter 2004.[95]

**Figure 11 — Thermogravimetric and derivative thermogravimetric curves for bacterial cellulose (solid line) and CNCs produced by sulfuric acid hydrolysis using conditions that give different numbers of surface sulfate half esters (decreasing sulfate content from left to right)**

Overall, a number of studies have reported similar results, with the surface modified cellulose starting to degrade at lower temperatures than the source cellulose and with a more complex thermogram.[90][161][167][168][169] The onset of degradation (ignoring the loss of residual water and/or other volatile compounds below 150 °C) is typically in the range of 190 °C to 220 °C for sulfated CNCs derived from wood pulp, cotton and bacterial celluloses, always significantly lower than the unhydrolyzed cellulose. Carboxylated CNCs have been reported to be more thermally stable with <5 % mass loss below ~220 °C to 270 °C for CNCs from a variety of sources.[16][19][52] However, this study did not include a direct comparison of TGA results for sulfated and carboxylated CNCs measured under identical conditions. Interestingly, the phosphorylated and uncharged CNCs produced by hydrolysis with phosphoric acid and HCl, respectively, also showed higher thermal stability (<5 % mass loss below 305 °C and 290 °C for phosphorylated and hydroxylated CNCs), a single well-defined decomposition step and low char content. By contrast, sulfated CNCs prepared from the same cellulose source gave a broad thermogram shifted to lower temperatures.[14] The surface phosphate content was ~4 mmol/g as compared to ~100 mmol/g for the sulfated CNCs, so the higher stability of the phosphorylated CNCs might be primarily due to the different concentration of charged surface groups.

Although most studies of thermal stability have used TGA, there are a few examples where differential scanning calorimetry (DSC) has been used as an alternate method for either CNCs or surface modified CNCs.[170][171][172] DSC is much more widely used for assessing changes in thermal properties for CNC nanocomposites, usually at lower temperatures than those used to measure the thermal degradation of CNCs.

The thermal expansion coefficient is an important property for consideration when CNCs are incorporated in nanocomposites. Although it can be measured experimentally for CNC films or composites, it is difficult to measure experimentally for individual CNCs. The few experimental determinations from the d-spacing measured by low temperature XRD indicate a low coefficient of thermal expansion (in the range of 5 ppm/K to 50 ppm/K) and have been supported by values obtained by simulations.[173][174][175] The same applies to the tensile strength of CNCs.[174]

## 8.2 Viscosity

The viscosity of CNC suspensions depends on the dimensions and surface properties of the nanocrystals. It has been suggested that, similarly to DLS, viscosity might provide a rapid method for routine characterization for commercial production of CNCs. The intrinsic viscosity, which measures the contribution of the suspended material to the viscosity of the suspending solution is typically measured, using either a capillary viscometer or a rolling ball viscometer. In these experiments, the relative viscosity of the suspension is measured over a range of CNC concentrations and the intrinsic viscosity is obtained by extrapolation of plots of relative viscosity vs concentration or reciprocal concentration (expressed as weight/volume), using one of several data treatment methods described in the literature. For wood pulp CNCs, two recent studies have reported intrinsic viscosities of 270 mL/g and 213 mL/g, with the differences in the values attributed to different dimensions, surface charge and counterion for the two samples.[132][176] A significantly different value was obtained for larger tunicate CNCs (1,03 dL/g; see Reference [177]) and increasing the ionic strength of the suspension by adding NaCl also affected the intrinsic viscosity.[132] As discussed in 5.3, intrinsic viscosity has also been used to assess the degree of polymerization of cellulosic nanomaterials, although in this case the method relies on completely dissolving the samples prior to analysis.

At low concentrations CNC suspensions have randomly oriented crystals; with increasing concentrations the rod-shaped CNCs first align to give an anisotropic nematic liquid-crystalline phase and at a critical concentration a chiral nematic phase forms. The formation of these ordered phases is responsible for the unique optical properties of CNC suspensions and films. Since the particle alignment is highly dependent on the shear rate, many studies have focused on measuring the viscosity as a function of shear rate (dynamic viscosity, units of Pa·s). Several studies have shown that the viscosity depends strongly on time, shear rate, and CNC counterion.[43][132][178] Most of these studies have used high concentrations of CNCs containing anisotropic phases or incorporated CNCs in other materials for modification of their rheological properties[160][162][179] and are thus beyond the scope of this Technical Report. Several reviews provide an overview of work in this area.[2][8][180]

## 9 Concluding comments

This Technical Report has summarized methods used to characterize CNCs with an emphasis on sample preparation, data acquisition and data analysis. The review of the current state-of-the-art for CNC characterization focuses on methods that are well-established and broadly applied. Alternate methods which have been shown to be useful for other types of nanomaterials have not been included, as their utility for CNCs has yet to be demonstrated.[181] These include particle sizing or fractionation methods, such as small angle X-ray diffraction, field flow fractionation or analytical ultracentrifugation and surface analysis methods, such as secondary ion mass spectrometry. However, other types of cellulose nanomaterials have been studied using some of these methods.[182][183][184][185] Also excluded are optical and mechanical properties, which are important parameters for thin film CNC samples and for CNC nanocomposite applications, but which are outside the scope of a review that focuses on properties of unmodified CNCs. The characterization of CNCs is a first step towards realizing the market potential for a wide variety of cellulose nanomaterial-enabled products.[4][5]

Recent workshop and task group reports have identified initial challenges for standardization of cellulosic nanomaterials<sup>[186][187]</sup> and in concluding it is useful to assess whether the characterization methods are sufficiently advanced for this purpose. For CNC composition, some methods are well-established (e.g. elemental analysis) or can be adapted with minor modifications from existing pulp and paper standards (e.g. cellulose biomass contaminants, degree of polymerization). The determination of surface sulfate half-esters for CNCs produced by sulfuric acid hydrolysis has been extensively studied and should be ready for standardization after an inter-laboratory comparison. The quantification of other surface functional groups produced during acid hydrolysis or post-production modification has been investigated although quantitative and reproducible measurements will require additional work. Crystallinity measurements vary significantly depending on the instrument and analysis method and will also require additional studies and comparisons before a standard approach can be recommended. Particle morphology (size distribution, aspect ratio) has been extensively examined using particle counting methods; microscopy measurements are subject to many of the same challenges that have been identified (and are being solved) for other nanomaterials, and it is likely that standard protocols can be developed and validated using an inter-laboratory comparison. Correlating particle counting data with ensemble methods, such as DLS that examine the bulk sample would be very valuable since DLS is a quicker and less expensive method for routine measurements and avoids the sampling issues encountered with microscopy. However, the difficulty of dealing with broad size distributions and non-spherical particles remains unresolved. It is possible that hybrid fractionation methods and/or multi-angle light scattering<sup>[188]</sup> might help to overcome the issues associated with DLS. Although standardizing primary particle size distributions might be possible in the near future, methods to assess agglomeration in colloidal suspensions (as prepared or after redispersion of dry CNCs) over a wide range of length scales are not well-developed. Estimates of surface charge using zeta potential are likely to be plagued by the same difficulties that have so far made it difficult to obtain repeatable values for round robin studies of other nanomaterials. Finally, surface area measurements used for other nanomaterials are not applicable to dry CNCs. Overall, one of the more pressing problems remains the lack of methods that can be used for rapid quality control in a manufacturing environment.<sup>[189]</sup>

## Bibliography

- [1] POSTEK M.T., MOON R.J., RUDIE A.W., BILODEAU M.A. eds. Production and applications of cellulose nanomaterials. TAPPI Press, Atlanta, GA, 2013
- [2] MOON R.J., MARTINI A., NAIRN J., SIMONSEN J., YOUNGBLOOD J. Cellulose nanomaterials review: structure, properties and nanocomposites. *Chem. Soc. Rev.* 2011, **40** pp. 3941–3994
- [3] DUFRESNE A. Nanocellulose: a new ageless bionanomaterial. *Mater. Today.* 2013, **16** pp. 220–227
- [4] SHATKIN J.A., WEGNER T.H., BILEK E.M., COWIE J. Market projections of cellulose nanomaterial-enabled products — Part 1: Applications. *Tappi J.* 2014, **13** pp. 9–16
- [5] FUTURE MARKETS INC. The global market for nanocellulose to 2020; Technology report no. 60, 2<sup>nd</sup> edition. Rockville, MD. ( 2013).
- [6] ISO 20477<sup>1)</sup>, *Nanotechnologies — Standard terms and their definition for cellulose nanomaterial*
- [7] EICHHORN S. Cellulose nanowhiskers: Promising materials for advanced applications. *Soft Matter.* 2011, **7** pp. 303–315
- [8] HABIBI Y., LUCIA L.A., ROJAS O.J. Cellulose nanocrystals: Chemistry, self-assembly and applications. *Chem. Rev.* 2010, **110** pp. 3479–3500
- [9] BRINCHI L., COTANA F., FORTUNATI E., KENNEY J.M. Production of nanocrystalline cellulose from lignocellulosic biomass: technology and applications. *Carbohydr. Polym.* 2013, **94** pp. 154–169
- [10] BRITO B.S.L., PEREIRA F.V., PUTAUX J.-L., JEAN B. Preparation, morphology and structure of cellulose nanocrystals from bamboo fibers. *Cellulose.* 2012, **19** pp. 1527–1536
- [11] CESAR N.R., PEREIRA-DA-SILVA M.A., BOTARO V.R., DE MENEZES A.J. Cellulose nanocrystals from natural fiber of the macrophyte *Typha domingensis*: Extraction and characterization. *Cellulose.* 2015, **22** pp. 449–460
- [12] CHAN C.H., CHIA C.H., ZAKARIA S., AHMAD I., DUFRESNE A. Production and characterization of cellulose and nanocrystalline cellulose from kenaf core wood. *BioResources.* 2013, **8** pp. 785–794
- [13] MARTINEZ-SANZ M., VICENTE A.A., GONTARD N., LOPEZ-RUBIO A., LAGARON J.M. On the extraction of cellulose nanowhiskers from food by-products and their comparative reinforcing effect on a polyhydroxybutyrate-co-valerate polymer. *Cellulose.* 2015, **22** pp. 535–551
- [14] ESPINOSA S.C., KUHN T., FOSTER E.J., WEDER C. Isolation of thermally stable cellulose nanocrystals by phosphoric acid hydrolysis. *Biomacromolecules.* 2013, **14** pp. 1223–1230
- [15] LIU Y., WANG H., YU G., YU Q., LI B., MU X. A novel approach for the preparation of nanocrystalline cellulose by using phosphotungstic acid. *Carbohydr. Polym.* 2014, **110** pp. 415–422
- [16] LEUNG A.C.W., HRAPOVIC S., LAM E., LIU Y., MALE K.B., MAHMOUD K.A. Characteristics and properties of carboxylated cellulose nanocrystals prepared from a novel one-step procedure. *Small.* 2011, **7** pp. 302–305
- [17] LU Q., TANG L., LIN F., WANG S., CHEN Y., CHEN X. Preparation and characterization of cellulose nanocrystals via ultrasonication-assisted FeCl<sub>3</sub>-catalyzed hydrolysis. *Cellulose.* 2014, **21** pp. 3497–3506
- [18] TANG L., HUANG B., LU Q., WANG S., OU W., LIN W. Ultrasonication-assisted manufacture of cellulose nanocrystals esterified with acetic acid. *Bioresour. Technol.* 2013, **127** pp. 100–105

---

1) Under preparation.

- [19] ARAKI J., WADA M., KUGA S. Steric stabilization of a cellulose microcrystal suspension by poly(ethylene glycol) grafting. *Langmuir*. 2001, **17** pp. 21–27
- [20] HEMRAZ U.D., BOLUK Y., SUNASEE R. Amine-decorated nanocrystalline cellulose surfaces: synthesis, characterization and surface properties. *Can. J. Chem.* 2013, **91** pp. 974–981
- [21] BECK-CANDANEDO S., ROMAN M., GRAY D.G. Effect of reaction conditions on the properties and behavior of wood cellulose nanocrystal suspensions. *Biomacromolecules*. 2005, **6** pp. 1048–1054
- [22] ELAZZOUZI-HAFRAOUI S., NISHIYAMA Y., PUTAUX J.-L., HEUX L., DUBREUILF F., ROCHAS C. The shape and size distribution of crystalline nanoparticles prepared by acid hydrolysis of native cellulose. *Biomacromolecules*. 2008, **9** pp. 57–65
- [23] KONTTURI E., & VUORINEN T. Indirect evidence of supramolecular changes within cellulose microfibrils of chemical pulp fibers upon drying. *Cellulose*. 2009, **16** pp. 65–74
- [24] RAMANEN P., PENTTILA P.A., SVEDSTROM K., MAUNU S.L., SERIMAA R. The effect of drying method on the properties and nanoscale structure of cellulose whiskers. *Cellulose*. 2012, **19** pp. 901–912
- [25] WANG Q., ZHAO X., ZHU J.Y. Kinetics of strong acid hydrolysis of a bleached kraft pulp for producing cellulose nanocrystals (CNCs). *Ind. Eng. Chem. Res.* 2014, **53** pp. 11007–11014
- [26] WANG Q.Q., ZHU J.Y., REINER R.S., VERRILL S.P., BAXA U., MCNEIL S.E. Approaching zero cellulose loss in cellulose nanocrystal (CNC) production: recovery and characterization of cellulosic solid residues (CSR) and CNC. *Cellulose*. 2012, **19** pp. 2033–2047
- [27] HAMAD W.Y., & HU T.Q. Structure-property-yield inter-relationships in nanocrystalline cellulose extraction. *Can. J. Chem. Eng.* 2010, **88** pp. 392–402
- [28] BECK S., BOUCHARD J., BERRY R. Dispersibility in water of dried nanocrystalline cellulose. *Biomacromolecules*. 2012, **13** pp. 1486–1494
- [29] DONG X.M., & GRAY D.G. Effect of counterions on ordered phase formation in suspensions of charged rodlike cellulose crystallites. *Langmuir*. 1997, **13** pp. 2404–2409
- [30] ABITBOL T., KLOSER E., GRAY D.G. Estimation of the surface sulfur content of cellulose nanocrystals prepared by sulfuric acid hydrolysis. *Cellulose*. 2013, **20** pp. 785–794
- [31] ISO 14887:2000, *Sample preparation - Dispersing procedures for powders in liquids*
- [32] TAUROZZI J.S., HACKLEY V.A., WIESNER M.R. Ultrasonic dispersion of nanoparticles for environmental, health and safety assessment - issues and recommendations. *Nanotoxicology*. 2011, **5** pp. 711–729
- [33] See order 2012-87-09-01 amending the Canadian Domestic Substances List: <http://www.gazette.gc.ca/rp-pr/p2/2012/2012-11-21/html/sor-dors229-eng.html>.
- [34] ISO 12805, *Nanotechnologies — Materials specifications — Guidance on specifying nano-objects*
- [35] *Cellulose, powdered*: European Pharmacopoeia. *Maisonneuve*. 2005, **5** p. 1232
- [36] STEFANIAK A.B., SEEHRA M.S., FIX N.R., LEONARD S.S. Lung biodurability and free radical production of cellulose nanomaterials. *Inhal. Toxicol.* 2014, **26** pp. 733–749
- [37] BECK S., MÉTHOT M., BOUCHARD J. General procedure for determining cellulose nanocrystal sulfate half-ester content by conductometric titration. *Cellulose*. 2015, **22** pp. 101–116
- [38] CSA Z5100, *Cellulosic nanomaterials: Test methods for characterization*
- [39] ARAKI J., WADA M., KUGA S., OKANO T. Influence of surface charge on viscosity behavior of cellulose microcrystal suspension. *J. Wood Sci.* 1999, **45** pp. 258–261

- [40] JIANG F., ESKER A.R., ROMAN M. Acid-catalyzed and solvolytic desulfation of H<sub>2</sub>SO<sub>4</sub>-hydrolyzed cellulose nanocrystals. *Langmuir*. 2010, **26** pp. 17919–17925
- [41] KATZ S., BEATSON R.P., SCALLAN A.M. The determination of strong and weak acidic groups in sulfite pulps. *Sven. Papperstidn.* 1984, **87** pp. R48–R53
- [42] HABIBI Y., CHANZY H., VIGNON M.R. TEMPO-mediated surface oxidation of cellulose whiskers. *Cellulose*. 2006, **13** pp. 679–687
- [43] ARAKI J., WADA M., KUGA S., OKANO T. Flow properties of microcrystalline cellulose suspension prepared by acid treatment of native cellulose. *Colloids Surf. A Physicochem. Eng. Asp.* 1998, **142** pp. 75–82
- [44] DONG X.M., REVOL J.-F., GRAY D.G. Effect of microcrystallite preparation conditions on the formation of colloid crystals of cellulose. *Cellulose*. 1998, **5** pp. 19–32
- [45] GU J., CATCHMARK J.M., KAISER E.Q., ARCHIBALD D.D. Quantification of cellulose nanowhiskers sulfate esterification levels. *Carbohydr. Polym.* 2013, **92** pp. 1809–1816
- [46] EDGAR C.D., & GRAY D.G. Smooth model cellulose I surfaces from nanocrystal suspensions. *Cellulose*. 2003, **10** pp. 299–306
- [47] HABIBI Y., GOFFIN A.-L., SCHILTZ N., DUQUESNE E., DUBOIS P., DUFRESNE A. Bionanocomposites based on poly(ε-caprolactone)-grafted cellulose nanocrystals by ring-opening polymerization. *J. Mater. Chem.* 2008, **18** pp. 5002–5010
- [48] ZOPPE J.O., RUOTTINEN V., RUOTSALAINEN J., RÖNKKÖ S., JOHANSSON L.-S., HINKKANEN A. Synthesis of cellulose nanocrystals carrying tyrosine sulfate mimetic ligands and inhibition of alphavirus infection. *Biomacromolecules*. 2014, **15** pp. 1534–1542
- [49] HAN J., ZHOU C., WU Y., LIU F., WU Q. Self-assembling behavior of cellulose nanoparticles during freeze-drying: effect of suspension concentration, particle size, crystal structure and surface charge. *Biomacromolecules*. 2013, **14** pp. 1529–1540
- [50] CASTRO-GUERRERO C.F., & GRAY D.G. Chiral nematic phase formation by aqueous suspensions of cellulose nanocrystals prepared by oxidation with ammonium persulfate. *Cellulose*. 2014, **21** pp. 2567–2577
- [51] DA SILVA PEREZ D., MONTANARI S., VIGNON M.R. TEMPO-Mediated Oxidation of Cellulose III. *Biomacromolecules*. 2003, **4** pp. 1417–1425
- [52] FILPPONEN I., & ARGYROPOULOS D.S. Regular linking of cellulose nanocrystals via click chemistry: Synthesis and formation of cellulose nanoplatelet gels. *Biomacromolecules*. 2010, **11** pp. 1060–1066
- [53] BATTISTA O.A., COPPICK S., HOWSMON J.A., MOREHEAD F.F., SISSON W.A. Level-off degree of polymerization. *Ind. Eng. Chem.* 1956, **48** pp. 333–335
- [54] HETTRICH K., PINNOW M., VOLKERT B., PASSAUER L., FISCHER S. Novel aspects of nanocellulose. *Cellulose*. 2014, **21** pp. 2479–2488
- [55] LAPIERRE L., & BOUCHARD J. Molecular weight determination of softwood kraft cellulose: effects of carbanilation solvent, hemicelluloses and lignin. In: *Advances in lignocellulosics characterization*, (ARGYROPOULOS D.S. ed.). TAPPI Press, Atlanta, GA, 2000, pp. 239–62.
- [56] NISHIYAMA Y., KIM U.-J., KIM D.-Y., KATSUMATA K.S., MAY R.P., LANGAN P. Periodic disorder along ramie cellulose microfibrils. *Biomacromolecules*. 2003, **4** pp. 1013–1017
- [57] HU T.Q., HASHAIKEH R., BERRY R.M. Isolation of a novel, crystalline cellulose material from the spent liquor of cellulose nanocrystals (CNCs). *Cellulose*. 2014, **21** pp. 3217–3229



- [58] KLOSER E., & GRAY D.G. Surface grafting of cellulose nanocrystals with poly(ethylene oxide) in aqueous media. *Langmuir*. 2010, **26** pp. 13450–13456
- [59] ISO 5351, *Pulps — Determination of limiting viscosity number in cupri-ethylenediamine (CED) solution*
- [60] ASTM D1795-13, *Standard test method for intrinsic viscosity of cellulose*
- [61] ASTM D4243-09, *Standard test method for measurement of average viscometric degree of polymerization of new and aged electrical papers and boards*
- [62] SJÖHOLM E., GUSTAFSSON K., ERIKSSON B., BROWN W., COLMSJÖ A. Aggregation of cellulose in lithium chloride/N,N-dimethylacetamide. *Carbohydr. Polym.* 2000, **41** pp. 153–161
- [63] XU F., SHI Y.-C., WANG D. X-ray scattering studies of lignocellulosic biomass: A review. *Carbohydr. Polym.* 2013, **94** pp. 904–917
- [64] PARK S., BAKER J.O., HIMMEL M.E., PARILLA P.A., JOHNSON D.K. Cellulose crystallinity index: measurement techniques and their impact on interpreting cellulase performance. *Biotechnol. Biofuels*. 2010, **3** p. 10
- [65] FOSTON M. Advances in solid-state NMR of cellulose. *Curr. Opin. Biotechnol.* 2014, **27** pp. 176–184
- [66] AGARWAL U.P., REINER R.S., RALPH S.A. Cellulose I crystallinity determination using FT-Raman spectroscopy: Univariate and multivariate methods. *Cellulose*. 2010, **17** pp. 721–733
- [67] SCHENZEL K., FISCHER S., BRENDLER E. New method for determining the degree of cellulose I crystallinity by means of FT Raman spectroscopy. *Cellulose*. 2005, **12** pp. 223–231
- [68] MOON R.J., PÖHLER T., TAMMELIN T. Microscopic characterization of nanofibres and nanocrystals. In: *Handbook of Green Materials: Processing Technologies, Properties and Applications*, (OKSMAN K., MATTHEW A.P., BISMARCK A., ROJAS O., SAIN M. eds.). World Scientific, Singapore, 2014, pp. 159–80.
- [69] THYGESEN A., ODDERSHEDE J., LILHOLT H., THOMSEN A.B., STAHL K. On the determination of crystallinity and cellulose content in plant fibres. *Cellulose*. 2005, **12** pp. 563–576
- [70] SEGAL L., CREELY J.J., MARTIN A.E., CONRAD C.M. An empirical method for estimating the degree of crystallinity of native cellulose using the x-ray diffractometer. *Text. Res.* 1959, **29** pp. 786–794
- [71] RULAND W. X-ray determination of crystallinity and diffuse disorder scattering. *Acta Crystallogr.* 1961, **14** pp. 1180–1185
- [72] LANGFORD J., & WILSON A. Scherrer after sixty years: A survey and some new results in the determination of crystallite size. *J. Appl. Cryst.* 1978, **11** pp. 102–113
- [73] SÈBE G., HAM-PICHAVENT F., IBARBOURE E., LYDIE A., KOFFI C., TINGAUT P. Supramolecular structure characterization of cellulose II nanowhiskers produced by acid hydrolysis of cellulose I substrates. *Biomacromolecules*. 2012, **13** pp. 570–578
- [74] BRIOIS B., SAITO T., PETRIER C., PUTAUX J.-L., NISHIYAMA Y., HEUX L. I<sub>α</sub>-I<sub>β</sub> transition of cellulose under ultrasonic radiation. *Cellulose*. 2013, **20** pp. 597–603
- [75] PAN J., HAMAD W., STRAUS S.K. Parameters affecting the chiral nematic phase of nanocrystalline cellulose films. *Biomacromolecules*. 2010, **43** pp. 3851–3858
- [76] NEWMAN R.H. Homogeneity in cellulose crystallinity between samples of *Pinus radiata* wood. *Holzforschung*. 2004, **58** pp. 91–96
- [77] ATALLA R.H., & VANDERHART D.L. The role of solid state <sup>13</sup>C NMR spectroscopy in studies of the nature of native celluloses. *Solid State Nucl. Magn. Reson.* 1999, **15** pp. 1–19

- [78] NEWMAN R.H., & HEMMINGSON J.A. Carbon- 13 NMR distinction between categories of molecular order and disorder in cellulose. *Cellulose*. 1994, **2** pp. 95–110
- [79] SACUI I.A., NIEUWENDAAL R.C., BURNETT D.J., STRANICK S.J., JORFI M., WEDER C. Comparison of the properties of cellulose nanocrystals and cellulose nanofibrils isolated from bacteria, tunicate and wood processed using acid, enzymatic, mechanical and oxidative methods. *ACS Appl. Mater. Interfaces*. 2014, **6** pp. 6127–6138
- [80] IDSTROM A., BRELID H., NYDÉN M., NORDSTIERNA L. CP/MAS <sup>13</sup>C NMR study of pulp hornification using nanocrystalline cellulose as a model system. *Carbohydr. Polym.* 2013, **92** pp. 881–884
- [81] NADA A.-A.M.A., KAMEL S., EL-SAKHAWY M. Thermal behaviour and infrared spectroscopy of cellulose carbamates. *Polym. Degrad. Stabil.* 2000, **70** pp. 347–355
- [82] SIROKY J., BLACKBURN R.S., BECHTOLD T., TAYLOR J., WHITE P. Attenuated total reflectance Fourier-transform Infrared spectroscopy analysis of crystallinity changes in lyocell following continuous treatment with sodium hydroxide. *Cellulose*. 2010, **17** pp. 103–115
- [83] NELSON M.L., & O'CONNOR R.T. Relation of certain infrared bands to cellulose crystallinity and crystal lattice type. Part II. A new infrared ratio for estimation of crystallinity in celluloses I and II. *J. Appl. Polym. Sci.* 1964, **8** pp. 1325–1341
- [84] KLJUN A., BENIANS T.A.S., GOUBET F., MEULEWAETER F., KNOX J.P., BLACKBURN R.S. Comparative analysis of crystallinity changes in cellulose I polymers using ATR-FTIR, X-ray diffraction and carbohydrate-binding module probes. *Biomacromolecules*. 2011, **12** pp. 4121–4136
- [85] HULLEMAN S.H.D., VAN HAZENDONK J.M., VAN DAM J.E.G. Determination of crystallinity in native cellulose from higher plants with diffuse reflectance Fourier transform infrared spectroscopy. *Carbohydr. Res.* 1994, **261** pp. 163–172
- [86] O'CONNOR R.T., DUPRE E.F., MITCHAM D. Applications of Infrared Absorption Spectroscopy to Investigations of Cotton and Modified Cottons. Part I: Physical and Crystalline Modifications and Oxidation. *Text. Res. J.* 1958, **28** pp. 382–392
- [87] AGARWAL U.P., REINER R.R., RALPH S.A. Estimation of cellulose crystallinity of lignocelluloses using near-IR FT-Raman spectroscopy and comparison of the Raman and Segal-WAXS methods. *J. Agric. Food Chem.* 2013, **61** pp. 103–113
- [88] AGARWAL U.P., REINER R.S., RALPH S.A. Crystallinity of nanocellulose materials by near-IR FT-Raman spectroscopy. In: Production and applications of cellulose materials, (POSTEK M.T., MOON R.J., RUDIE A.J., BILODEAU M.A. eds.). TAPPI Press, Atlanta, 2013, pp. 43–4.
- [89] HAYASHI N., KONDO T., ISHIHARA M. Enzymatically produced nano-ordered short elements containing cellulose Ib crystalline domains. *Carbohydr. Polym.* 2005, **61** pp. 191–197
- [90] JIANG F., & HSIEH Y.-L. Chemically and mechanically isolated nanocellulose and their self-assembled structures. *Carbohydr. Polym.* 2013, **95** pp. 32–40
- [91] HABIBI Y., HOEGER I., KELLEY S.S., ROJAS O.J. Development of Langmuir-Schaeffer cellulose nanocrystal monolayers and their interfacial behaviors. *Langmuir*. 2009, **26** pp. 990–1001
- [92] CATETO C.A., & RAGAUSKAS A. Amino acid modified cellulose whiskers. *RSC Advances*. 2011, **1** pp. 1695–1697
- [93] MABROUK A.B., FERRARIA A.M., BOTELHJO DO ROGO A.M., BOUFI S. Highly transparent nanocomposite films based on polybutylmethacrylate and functionalized cellulose nanocrystals. *Cellulose*. 2013, **20** pp. 1711–1723
- [94] Cellulose Nanocrystal Reference Material Certificate, National Research Council Canada. 2014)
- [95] ROMAN M., & WINTER W.T. Effect of sulfate groups from sulfuric acid hydrolysis on the thermal degradation behavior of bacterial cellulose. *Biomacromolecules*. 2004, **5** pp. 1671–1677

- [96] BECK S., & BOUCHARD J. Effect of storage conditions on cellulose nanocrystal stability. *Tappi J.* 2014, **13** pp. 53–61
- [97] ISO 638, *Paper, board and pulps — Determination of dry matter content — Oven-drying method*
- [98] TAPPI T249 cm-09, *Carbohydrate composition of extractive-free wood and wood pulp by gas-liquid chromatography*
- [99] SULLIVAN J., & DOUEK M. Determination of carbohydrates in wood, pulp and process liquor samples by high-performance anion-exchange chromatography with pulsed amperometric detection. *J. Chromatogr. A.* 1994, **671** pp. 339–350
- [100] Paptac G18. 2007, *Kappa number of pulp*
- [101] TAPPI T204 cm-07, *Solvent extractives of wood and pulp*
- [102] VASSILEVA E., & QUETEL C.R. Certification measurement of the cadmium, copper and lead contents in rice using isotope dilution inductively coupled plasma mass spectrometry. *Anal. Chim. Acta.* 2004, **519** pp. 79–86
- [103] YANG L., MESTER Z., STURGEON R.E. Improvement in measurement precision with SPME by use of isotope dilution mass spectrometry and its application to the determination of tributyltin in sediment using SPME GC-ICP-MS. *J. Anal. At. Spectrom.* 2002, **17** pp. 944–949
- [104] WATTERS R.L., EBERHARDT K.R., BEARY E.S., FASSET J.D. Protocol for isotope dilution using inductively coupled plasma mass spectrometry for the determination of inorganic elements. *Metrologia.* 1997, **34** pp. 87–96
- [105] LABET M., & THIELEMANS W. Improving the reproducibility of chemical reactions on the surface of cellulose nanocrystals: ROP of  $\epsilon$ -caprolactone as a case study. *Cellulose.* 2011, **18** pp. 607–617
- [106] LIU P., SEHAQUI H., TINGAUT P., WICHSER A., OKSMAN K., MATHEW A.P. Cellulose and chitin nanomaterials for capturing silver ions ( $\text{Ag}^+$ ) from water via surface adsorption. *Cellulose.* 2014, **21** pp. 449–461
- [107] JOHANSSON L.-S., & CAMPBELL J.M. Reproducible XPS on biopolymers: cellulose studies. *Surf. Interface Anal.* 2004, **36** pp. 1018–1022
- [108] ISO 14187:2011, *Surface Chemical Analysis – Characterization of nanostructured materials*
- [109] SHARD A.G. Detection limits in XPS for more than 6000 binary systems using Al and Mg K $\alpha$  X-rays. *Surf. Interface Anal.* 2014, **46** pp. 175–185
- [110] ZOPPE J.O., HABIBI Y., ROJAS O.J., VENDITTI R.A., JOHANSSON L.-S., EFIMENKO K. Poly(N-isopropylacrylamide) brushes grafted from cellulose nanocrystals via surface-initiated single electron transfer living radical polymerization. *Biomacromolecules.* 2010, **11** pp. 2683–2691
- [111] CRANSTON E.D., & GRAY D.G. Morphological and optical characterization of polyelectrolyte multilayers incorporating nanocrystalline cellulose. *Biomacromolecules.* 2006, **7** pp. 2522–2530
- [112] KAUSHIK M., CHEN W.C., VAN DE VEN T.G.M., MOORE A. An improved methodology for imaging cellulose nanocrystals by transmission electron microscopy. *Nord. Pulp Paper Res. J.* 2014, **29** pp. 77–84
- [113] KVIEN I., TANEM B.S., OSMAN K. Characterization of cellulose whiskers and their nanocomposites by atomic force and electron microscopy. *Biomacromolecules.* 2005, **6** pp. 3160–3165
- [114] PENG Y., GARDNER D.J., HAN Y. Drying cellulose nanofibrils: in search of a suitable method. *Cellulose.* 2012, **19** pp. 91–102
- [115] MAJOINEN J., WALTHER A., MCKEE J.R., KONTTURI E., ASEYEV V., MALHO J.M. Polyelectrolyte brushes grafted from cellulose nanocrystals using Cu-mediated surface-initiated controlled radical polymerization. *Biomacromolecules.* 2011, **12** pp. 2997–3006

- [116] FRASCHINI C., CHAUVE G., LE BERRE J.-F., ELLIS S., MÉTHOT M., O'CONNOR B. Critical discussion of light scattering and microscopy techniques for CNC particle sizing. *Nordic Pulp & Paper J.* 2014, **29** pp. 31–40
- [117] ISO 29301, *Microbeam analysis — Analytical transmission electron microscopy — Methods for calibrating image magnification by using reference materials having periodic structures*
- [118] MAEDA H. An atomic force microscopy study for the assembly structures of tobacco mosaic virus and their size evaluation. *Langmuir.* 1997, **13** pp. 4150–4161
- [119] POSTEK M.T., VLADAR A., DAGATA J., FARKAS N., MING B., WAGNER R. Development of the metrology and imaging of cellulose nanocrystals. *Meas. Sci. Technol.* 2011, **22** p. 024005
- [120] POSTEK M.T., VLADAR A., DAGATA J., FARKAS N., MING B., SABO R. Cellulose nanocrystals the next big nano-thing?”, *SPIE Proceedings*, 7042, 70420-70412 ( 2008)
- [121] KONTTURI E., JOHANSSON L.-S., KONTTURI K.S., AHONEN P., THIÛNE P.C., LAINE J. Cellulose nanocrystal submonolayers by spin coating. *Langmuir.* 2007, **23** pp. 9674–9680
- [122] ASTM E2530-06:2006, *Standard practice for calibrating the z-magnification of an atomic force microscope at subnanometer displacement levels using Si (111) monatomic steps*
- [123] ASTM E2859-11:2012, *Standard guide for size measurement of nanoparticles using atomic force microscopy*
- [124] ISO 11952, *Surface chemical analysis — Scanning probe microscopy — Determination of geometric quantities using SPM: Calibration of measuring systems*
- [125] GROBELNY J., DELRIO F. W., PRADEEP N., KIM D.-I., HACKLEY V. A., COOK R. F. Size measurement of nanoparticles using atomic force microscopy”, *National Institute of Standards and Technology and Nanotechnology Characterization Laboratory Protocol PCC-6*, Ver 1.1, ( 2009)
- [126] BRINKMANN A., CHEN M., COUILLARD M., JAKUBEK Z., LENG T., JOHNSTON L.J. Correlating cellulose nanocrystal particle size and surface area. *Biomacromolecules.* 2016, submitted
- [127] ISO 9276-6, *Representation of results of particle size analysis — Part 6: Descriptive and quantitative representation of particle shape and morphology*
- [128] ISO 13322-1, *Particle size analysis — Image analysis methods — Part 1: Static image analysis methods*
- [129] ISO 14488, *Particulate materials — Sampling and sample splitting for the determination of particulate properties*
- [130] ASTM E2578-07, *Standard practice for calculation of mean sizes/diameters and standard deviations of particle size distributions*
- [131] LAHIJI R.R., XU X., REIFENBERGER R., RAMAN A., RUDIE A., MOON R.J. Atomic force microscopy characterization of cellulose nanocrystals. *Langmuir.* 2010, **26** pp. 4480–4488
- [132] BOLUK Y., LAHIJI R., ZHAO L., MCDERMOTT M.T. Suspension viscosities and shape parameter of cellulose nanocrystals (CNC). *Coll. Surf. A.* 2011, **377** pp. 297–303
- [133] SIQUEIRA G., BRAS J., DUFRESNE A. Cellulose whiskers versus microfibrils: Influence of the nature of the nanoparticle and its surface functionalization on the thermal and mechanical properties of nanocomposites. *Biomacromolecules.* 2009, **10** pp. 425–432
- [134] ISO 22412, *Particle size analysis — Dynamic light scattering (DLS)*
- [135] ASTM E2490-09, *Standard guide for measurement of particle size distribution of nanomaterials in suspension by photon correlation spectroscopy (PCS)*

- [136] HACKLEY V. A., & CLOGSTON J. D. Measuring the size of nanoparticles in aqueous media using batch-mode dynamic light scattering”, *National Institute of Standards and Technology and Nanotechnology Characterization Laboratory Joint Assay Protocol*, PCC-1, ( 2007)
- [137] JAMTING A.K., CULLEN J., COLEMAN V.A., LAWN M., HERMANN J., MILES J. Systematic study of bimodal suspensions of latex nanoparticles using dynamic light scattering. *Adv. Powder Technol.* 2011, **22** pp. 290–293
- [138] FILIPE V., HAWE A., JISKOOT W. Critical evaluation of nanoparticle tracking analysis (NTA) by nanosight for the measurement of nanoparticles and protein aggregates. *Pharm. Res.* 2010, **27** pp. 796–810
- [139] DONG S., HIRANI A., COLACHINO K. R., LEE Y. W., ROMAN M. Cytotoxicity and cellular uptake of cellulose nanocrystals”, *Nano LIFE*, 2, 1241006-1241001-1241011 ( 2012)
- [140] YANAMALA N., FARCAS M.T., HATFIELD M.K., KISIN E.R., KAGAN V.E., GERACI C.L. In vivo evaluation of the pulmonary toxicity of cellulose nanocrystals: A renewable and sustainable nanomaterial of the future. *ACS Sustain. Chem. & Eng.* 2014, **2** pp. 1691–1698
- [141] de SOUZA LIMA M.M., WONG J.T., PAILLET M., BORSALI R., PECORA R. Translational and rotational dynamics of rodlike cellulose whiskers. *Langmuir.* 2003, **19** pp. 24–29
- [142] GUAN X., CUETO R., RUSSO P., QI Y., WU Q. Asymmetric flow field-flow fractionation with multiangle light scattering detection for characterization of cellulose nanocrystals. *Biomacromolecules.* 2012, **13** pp. 2671–2679
- [143] BRAUN B., DORGAN J.R., CHANDLER J.P. Cellulosic nanowhiskers. Theory and application of light scattering from polydisperse spheroids in the Rayleigh-Gans-Debye regime. *Biomacromolecules.* 2008, **9** pp. 1255–1263
- [144] URENA-BENAVIDES E.E., & KITCHENS C.L. Static light scattering of triaxial nanoparticle suspensions in the Rayleigh-Gans-Debye regime: Application to cellulose nanocrystals. *RSC Advances.* 2012, **2** pp. 1096–1105
- [145] BOLUK Y., & DANUMAH C. Analysis of cellulose nanocrystal rod lengths by dynamic light scattering and electron microscopy. *J. Nanopart. Res.* 2014, **16** p. 2174
- [146] DONG X.M., KIMURA T., REVOL J.-F., GRAY D.G. Effects of ionic strength on the isotropic-chiral nematic phase transition of suspensions of cellulose crystallites. *Langmuir.* 1996, **12** pp. 2076–2082
- [147] ISO 9277, *Determination of the specific surface area of solids by gas adsorption — BET method*
- [148] LINSINGER T., ROEBBEN G., GILLILAND D., CALZOLAI L., ROSSI F., GIBSON N. Requirements on measurements for the implementation of the European Commission definition of the term “nanomaterial” EUR Report 25404 EN. Europe Union, Luxembourg, ( 2012)
- [149] WEIBEL A., BOUCHET R., BOULC’H F., KNAUTH P. The big problem of small particles: A comparison of methods for determination of particle size in nanocrystalline anatase powders. *Chem. Mater.* 2005, **17** pp. 2378–2385
- [150] HEATH L., & THIELEMANS W. Cellulose nanowhisiker aerogels. *Green Chem.* 2012, **12** pp. 1448–1453
- [151] OUGIYA H., HIOKI N., WATANABE K., MORINAGA Y., YOSHINAGA F., SAMEJIMA M. Relationship between the physical properties and surface area of cellulose derived from adsorbates of various molecular sizes. *Biosci. Biotechnol. Biochem.* 1998, **62** pp. 1880–1884
- [152] GOODRICH J.D., & WINTER W.T.  $\alpha$ -Chitin nanocrystals prepared from shrimp shells and their specific surface area measurements. *Biomacromolecules.* 2007, **8** pp. 252–257

- [153] LARSSON P.T., SVENSON A., WÄGGERG L. A new, robust method for measuring average fibre wall pore sizes in cellulose I rich plant fibre walls. *Cellulose*. 2013, **20** pp. 623–631
- [154] CHUNILALL V., BUSH T., LARSSON P.T., IVERSON T., KINDNESS A. A CP/MAS <sup>13</sup>C-NMR study of cellulose fibril aggregation in eucalyptus dissolving pulps during drying and the correlation between aggregate dimensions and chemical reactivity. *Holzforschung*. 2010, **64** pp. 693–698
- [155] COOPER C.L., COSGROVE T., VAN DUIJNEVELDT J.S., MURRAY M., PRESCOTT S.W. The use of solvent relaxation NMR to study colloidal suspensions. *Soft Matter*. 2013, **9** pp. 7211–7228
- [156] ISO 13099-2, *Colloidal systems — Methods for zeta potential determination — Part 2: Optical methods*
- [157] ISO 13099-1, *Colloidal systems — Methods for zeta potential determination — Part 1: Electroacoustic and electrokinetic phenomena*
- [158] ASTM E2865-12, *Standard guide for measurement of electrophoretic mobility and zeta potential of nanosized biological materials*
- [159] CLOGSTON J. D. Measuring zeta potential of nanoparticles”, *Nanotechnology Characterization Lab Protocol. PCC-2*, ( 2009)
- [160] BOLUK Y., ZHAO L., INCANI V. Dispersions of nanocrystalline cellulose in aqueous polymer solutions: Structure formation of colloidal rods. *Langmuir*. 2012, **28** pp. 6114–6123
- [161] de MORAIS TEIXEIRA E., CORREA A.C., MANZOLI A., de LIMA LEITE F., de OLIVEIRA C.R., MATTOSO L.H.C. Cellulose nanofibers from white and naturally colored cotton fibers. *Cellulose*. 2010, **17** pp. 595–606
- [162] HASANI M., CRANSTON E.D., WESTMAN G., GRAY D.G. Cationic surface functionalization of cellulose nanocrystals. *Soft Matter*. 2008, **4** pp. 2238–2244
- [163] ASTM E1131-08, *Standard test method for compositional analysis by thermogravimetry*
- [164] ASTM E2040-08, *Standard test method for mass scale calibration of thermogravimetric analyzers*
- [165] ISO 11308, *Nanotechnologies — Characterization of single-wall carbon nanotubes using thermogravimetric analysis*
- [166] ISO 11358-1, *Plastics — Thermogravimetry (TG) of polymers — Part 1: General principles*
- [167] HOSSAIN K.M.Z., JASMANI L., AHMED I., PARSONS A.J., SCOTCHFORD C.A., THIELEMANS W. High cellulose nanowhisker content composites through cellosize bonding. *Soft Matter*. 2012, **8** pp. 12099–12110
- [168] KAN K.H.M., LI J., WIJESSEKERA K., CRANSTON E.D. Polymer-grafted cellulose nanocrystals as pH-responsive reversible flocculants. *Biomacromolecules*. 2013, **14** pp. 3130–3139
- [169] PETERSSON L., KVIEN I., OKSMAN K. Structure and thermal properties of poly(lactic acid)/cellulose whiskers nanocomposite materials. *Comp. Sci. Tech*. 2007, **67** pp. 2535–2544
- [170] UETANI K., WATANABE Y., ABE K., YANO H. Influence of drying method and precipitated salts on pyrolysis for nanocelluloses. *Cellulose*. 2014, **21** pp. 1631–1639
- [171] WANG N. Ding, E. and Cheng, R. “Thermal degradation behaviors of spherical cellulose nanocrystals with sulfate groups. *Polymer (Guildf)*. 2007, **48** pp. 3486–3493
- [172] SALAN A., LUCIA L.A., JAMEEL H. Fluorine-based surface decorated cellulose nanocrystals as potential hydrophobic and oleophobic materials. *Cellulose*. 2015, **22** pp. 397–406
- [173] DIAZ J.A., WU X., MARTINI A., YOUNGBLOOD J.P., MOON R.J. Thermal expansion of self-organized and shear-oriented cellulose nanocrystal films. *Biomacromolecules*. 2013, **14** pp. 2900–2908

- [174] WU X., MOON R.J., MARTINI A. Tensile strength of I $\beta$  crystalline cellulose predicted by molecular dynamics simulation. *Cellulose*. 2014, **21** pp. 2233–2245
- [175] HORI R., & WADA M. The thermal expansion of wood cellulose crystals. *Cellulose*. 2005, **12** pp. 479–484
- [176] GONZALEZ-LABRADA E., & GRAY D.G. Viscosity measurements of dilute aqueous suspensions of cellulose nanocrystals using a rolling ball viscometer. *Cellulose*. 2012, **19** pp. 1557–1565
- [177] BERCEA M., & NAVARD P. Shear dynamics of aqueous suspensions of cellulose whiskers. *Macromolecules*. 2000, **33** pp. 6011–6016
- [178] ORTS W.J., GODBOUT L., MARCHESSAULT R.H., REVOL J.-F. Enhanced ordering of liquid crystalline suspensions of cellulose microfibrils: A small angle neutron scattering study. *Macromolecules*. 1998, **31** pp. 5717–5725
- [179] URENA-BENAVIDES E.E., AO G., DAVIS V.A., KITCHENS C.L. Rheology and phase behavior of lyotropic cellulose nanocrystal suspensions. *Macromolecules*. 2011, **44** pp. 8990–8998
- [180] DE SOUSA LIMA M.M., & BORSALI R. Rodlike cellulose microcrystals: Structure, properties and applications. *Macromol. Rapid Commun*. 2004, **25** pp. 771–787
- [181] RAUSCHER H., ROEBBEN G., AMENTA V., BOIX SANFELIU A., CALZOLAI L., EMONS H., GAILLARD C., GIBSON N., LINSINGER T., MECH A., QUIROS PESUDO L., RASMUSSEN K., RIEGO SINTES J., SOKULL-KLÜTTGEN B., STAMM H. Towards a review of the EC Recommendation for a definition of the term “nanomaterial. Part 1: Compilation of information concerning the experience with the definition”, *European Commission Report* ( 2014)
- [182] JUNG S., FOSTON M., KALLURI U.C., TUSKAN G.A., RAGAUSKAS A.J. 3D Chemical image using TOF-SIMS revealing the biopolymer component spatial and lateral distributions in biomass. *Angew. Chem. Int. Ed*. 2012, **51** pp. 12005–12008
- [183] KENNEDY C.J., ŠTURCOVÁ A., JARVIS M.C., WESS T.J. Hydration effects on spacing of primary-wall cellulose microfibrils: A small angle X-ray scattering study. *Cellulose*. 2007, **14** pp. 410–408
- [184] MISSOUM K., BELGACEM M.N., BARNES J.-P., BROCHIER-SALON M.-C., BRAS J. Nanofibrillated cellulose surface grafting in ionic liquid. *Soft Matter*. 2012, **8** pp. 8338–8349
- [185] PENTTILÄ P.A., VÁRNAI A., FERNÁNDEZ M., KONTRO I., LILJESTRÖM V., LINDNER P. Small-angle scattering study of structural changes in the microfibril network of nanocellulose during enzymatic hydrolysis. *Cellulose*. 2013, **20** pp. 1031–1040
- [186] ISO/TC 6 Ad Hoc Group Report. Recommendations for the development of standards on the measurement and characterization of cellulosic nanomaterials ( 2014)
- [187] DAVIS C.S., MOON R.J., IRELAND S., FOSTER E.J., JOHNSTON L.J., SHATKIN J.A. NIST-TAPPI Workshop on Measurement Needs for Cellulose Nanomaterials. DOI: ( 2015)10.6028/NIST.SP.1192
- [188] BROWN S.C., BOYKO V., MEYERS G., VOETZ M., WOHLLEBEN W. Toward advancing nano-object count metrology: A best practice framework. *Environ. Health Perspect*. 2013, **121** pp. 1282–1291
- [189] POSTEK M.T. Nanomanufacturing metrology for cellulosic nanomaterials: An update”, *SPIE Proceedings*, 9173, 917302 ( 2014)

